Journal of Experimental Botany
https://doi.org/10.1093/jxb/erab409 Advance Access Publication 6 September, 2021

RESEARCH PAPER

Arabidopsis PAP17 is a dual-localized purple acid phosphatase up-regulated during phosphate deprivation, senescence, and oxidative stress

Bryden O'Gallagher[1], Mina Ghahremani[1,*], Kyla Stigter[1], Emma J.L. Walker[1,†], Michal Pyc[2,‡], Ang-Yu Liu[3], Gustavo C. MacIntosh[3], Robert T. Mullen[2] and William C. Plaxton[1,§]

[1] Department of Biology, Queen's University, Kingston, Ontario K7L 3N6, Canada
[2] Department of Molecular and Cellular Biology, University of Guelph, Guelph, Ontario N1G 2W1, Canada
[3] Roy J. Carver Department of Biochemistry, Biophysics and Molecular Biology, Iowa State University, Ames, IA 50011-1079, USA

* Present address: Public Health Agency of Canada,130 Colonnade Rd, A.L. 6501H, Ottawa, Ontario K1A 0K9, Canada.
† Present address: Department of Biochemistry, Western University, London, Ontario N6A 5C1, Canada.
‡ Present address: Willow Biosciences, Burnaby, British Columbia V5M 3Z3, Canada.
§ Correspondence: plaxton@queensu.ca

Received 4 June 2021; Editorial decision 3 September 2021; Accepted 5 September 2021

Editor: Nick Smirnoff, University of Exeter, UK

Abstract

A 35 kDa monomeric purple acid phosphatase (APase) was purified from cell wall extracts of Pi starved (–Pi) *Arabidopsis thaliana* suspension cells and identified as AtPAP17 (At3g17790) by mass spectrometry and N-terminal microsequencing. AtPAP17 was *de novo* synthesized and dual-localized to the secretome and/or intracellular fraction of –Pi or salt-stressed plants, or senescing leaves. Transiently expressed AtPAP17–green fluorescent protein localized to lytic vacuoles of the Arabidopsis suspension cells. No significant biochemical or phenotypical changes associated with AtPAP17 loss of function were observed in an *atpap17* mutant during Pi deprivation, leaf senescence, or salinity stress. Nevertheless, AtPAP17 is hypothesized to contribute to Pi metabolism owing to its marked up-regulation during Pi starvation and leaf senescence, broad APase substrate selectivity and pH activity profile, and rapid repression and turnover following Pi resupply to –Pi plants. While AtPAP17 also catalyzed the peroxidation of luminol, which was optimal at pH 9.2, it exhibited a low V_{max} and affinity for hydrogen peroxide relative to horseradish peroxidase. These results, coupled with absence of a phenotype in the salt-stressed or –Pi *atpap17* mutant, do not support proposals that the peroxidase activity of AtPAP17 contributes to the detoxification of reactive oxygen species during stresses that trigger AtPAP17 up-regulation.

Keywords: Hydrogen peroxide metabolism, peroxidase, phosphate metabolism, phosphate starvation response, purple acid phosphatase, reactive oxygen species, salinity stress, senescence.

Abbreviations: APase, acid phosphatase;AtPAP, *Arabidopsis thaliana* purple acid phosphatase;CW, cell wall;GFP, green fluorescent protein;H_2O_2, hydrogen peroxide;HMW, high molecular weight;HRP, horseradish peroxidase;LMW, low molecular weight;PAP, purple acid phosphatase;PEP, phosphoenolpyruvate;Po, organic-P;PRx, peroxidase;PSI, Pi starvation-inducible;PSR, Pi starvation response;qRT-PCR, quantitative real-time PCR;ROS, reactive oxygen species.

Introduction

Acid phosphatases (APases; EC 3.1.3.2) catalyze the hydrolysis of orthophosphate (Pi) from a wide variety of Pi monoesters and anhydrides with an acidic pH optimum. While Pi metabolism is essential during the entire lifespan of a plant, the mechanisms that drive Pi acquisition and use are of particular importance during nutritional Pi deprivation, a common stress that frequently limits plant growth in natural soils. Up-regulation of intracellular and secreted APase activity is a hallmark of the plant Pi starvation response (PSR) and leaf senescence (Tran *et al.*, 2010*a*; Robinson *et al.*, 2012*a*; Shane *et al.*, 2014; Wang and Liu, 2018; Dissanayaka *et al.*, 2021). The largest and most important class of plant Pi starvation- and senescence-inducible APases are the purple APases (PAPs) (Tran *et al.*, 2010*a*; Wang and Liu, 2018). PAPs belong to a binuclear metallohydrolase family that require heterovalent Fe^{3+}–M^{2+} catalytic centers (M=Fe, Zn, or Mn). Although primary PAP structures vary extensively, domains involved in formation of their bimetallic active site are highly conserved, with the pair of metal ions coordinated by seven invariant residues (Schenk *et al.*, 2013). Their characteristic purple or pink color arises from a charge transfer interaction between a metal-coordinating tyrosine residue and the ferric iron (Fe^{3+}) atom within the active site (Schenk *et al.*, 2013).

Several mammalian and plant PAPs have been characterized as bifunctional enzymes that catalyze both phosphatase and peroxidation reactions. The peroxidase (PRx) activity of mammalian PAPs arises from their redox-active ferrous iron (Fe^{2+}) that endows them with the ability to evolve or scavenge reactive oxygen species (ROS) through a Fenton-type reaction (Fig. 1) (Schenk *et al.*, 2013). Two genes encoding PAPs have been identified in the human genome, but only one (HsACP5) has been studied to date (see Supplementary Fig. S1) (Flanagan *et al.*, 2006; Schenk *et al.*, 2013). HsACP5's physiological functions include the conversion of hydrogen peroxide (H_2O_2) into highly reactive hydroxyl radicals that contribute to bone resorption and immune responses (Hayman and Cox, 1994; Schenk *et al.*, 2013). Similarly, the PRx activity of several plant PAPs was hypothesized to contribute to ROS detoxification during salinity and other oxidative stresses, or ROS production during leaf senescence or pathogen attack (del Pozo *et al.*, 1999; Liao *et al.*, 2003; Bozzo *et al.*, 2004*a*; Veljanovski *et al.*, 2006; Li *et al.*, 2008). The increased tolerance to oxidative damage of salt-stressed tobacco (*Nicotiana tabacum*) suspension cells and Arabidopsis plants overexpressing GmPAP3, a high molecular weight (HMW) soybean PAP, supports this hypothesis (Li *et al.*, 2008). Nevertheless, the mechanistic details that might allow PAPs to scavenge ROS remain obscure and await further investigations (Schenk *et al.*, 2013).

Our most comprehensive understanding of plant PAPs has arisen from studies of the Arabidopsis PAP (AtPAP) family, in which 29 *PAP* genes were annotated and classified into three phylogenetic groups according to their deduced primary

$$Fe^{3+}\text{–}Fe^{2+} + H_2O_2 \longrightarrow Fe^{3+}\text{–}Fe^{3+} + OH\bullet + OH^- \quad (1)$$

$$Fe^{3+}\text{–}Fe^{3+} + O_2^{\bullet -} \longrightarrow Fe^{3+}\text{–}Fe^{2+} + O_2 \quad (2)$$

Fig. 1. The Fenton reaction endows PAPs with peroxidation activity. The redox-active ferrous iron (Fe^{2+}) of the dinuclear active site of LMW mammalian PAPs generates highly reactive hydroxyl radicals (Equation 1) which play a key role in bone reabsorption and immune responses (Schenk *et al.*, 2013). In the reverse direction, the Fenton reaction can scavenge ROS (i.e. superoxide, $O_2^{\bullet -}$) to produce oxygen (Equation 2).

structures (Li *et al.*, 2002). Groups I and II comprise HMW PAPs, whereas Group III consists of low molecular weight (LMW) PAPs that are more closely related to mammalian PAPs than to HMW PAPs (Supplementary Fig. S1) (Schenk *et al.*, 2000, 2013). The evolution of HMW and LMW PAPs was a very early event, probably occurring before the plant–animal divergence (Li *et al.*, 2002; Tran *et al.*, 2010*a*). Several reports have described the up-regulation of specific vacuolar or secreted AtPAP isozymes during Pi deficiency, namely the HMW and closely related AtPAP10, AtPAP12, AtPAP25, and AtPAP26 (Supplementary Fig. S1), along with the LMW and distantly related AtPAP17 (del Pozo *et al.*, 1999; Veljanovski *et al.*, 2006; Tran *et al.*, 2010*b*; Wang *et al.*, 2011, 2014; Robinson *et al.*, 2012*a*, *b*; Del Vecchio *et al.*, 2014). Integrated biochemical and genetic approaches have identified AtPAP12 and AtPAP26 as the principal APases that are up-regulated and secreted by Pi-starved (–Pi) Arabidopsis to scavenge Pi from the soil's organic-P (Po) pool, or from cytoplasmic Po compounds that have leaked through the plasma membrane into the surrounding cell wall (CW) and apoplast (Veljanovski *et al.*, 2006; Hurley *et al.*, 2010; Robinson *et al.*, 2012*b*; Wang *et al.*, 2014; Ghahremani *et al.*, 2019*b*). The dual-localized AtPAP26 also functions as the predominant APase that participates in vacuolar and extracellular Pi recycling from Po compounds during Pi deprivation or leaf senescence (Hurley *et al.*, 2010; Robinson *et al.*, 2012*a*; Shane *et al.*, 2014; Wang *et al.*, 2014).

AtPAP17 was the first LMW or Pi starvation-inducible (PSI) AtPAP isozyme to be studied. del Pozo *et al.* (1999) purified a 35 kDa APase from the soluble intracellular fraction of hydroponic cultures of –Pi Arabidopsis seedlings and identified it as AtPAP17 (At3g17790, previously designated as AtACP5) by N-terminal sequencing. Although AtPAP17 exhibited APase and PRx activities (del Pozo *et al.*, 1999), kinetic studies of either activity have not been undertaken. While predicted to be a secreted protein (del Pozo *et al.*, 1999), AtPAP17's subcellular location also remains to be determined. Owing to the marked induction of *AtPAP17* mRNA in shoots and roots during Pi deprivation (del Pozo *et al.*, 1999), *AtPAP17* transcription has been frequently exploited as a positive control for studies of the Arabidopsis PSR (see, for example, Müller *et al.*, 2004; Veljanovski *et al.*, 2006; Tran and Plaxton, 2008; Hurley *et al.*, 2010). *AtPAP17* expression is also strongly induced in response to abscisic acid, salinity, or oxidative stress, as well as during leaf senescence (del Pozo *et al.*, 1999; Robinson *et al.*, 2012*a*). Together with its PRx activity, this led to the hypothesis that

AtPAP17 functions in ROS metabolism, in addition to its potential role in Pi scavenging and recycling (del Pozo *et al.*, 1999). A recent report described the involvement of *AtPAP17* and *AtPAP26* genes in an 'Arabidopsis Pi compensation network', such that loss of expression of one of them was buffered by the up-regulation of the other isozyme (Farhadi *et al.*, 2020).

The present study describes the purification and physical, kinetic, and molecular characterization of AtPAP17 from CW extracts of –Pi Arabidopsis cell cultures. Evidence that AtPAP17 is up-regulated and dual-localized to the extracellular matrix and cell vacuole of –Pi or salt-stressed Arabidopsis is also presented. A reverse genetics approach allowed us to evaluate AtPAP17 function during Pi deprivation, leaf senescence, and salinity stress by comparing the phenotype of an *atpap17* T-DNA insertional mutant with that of wild-type (Col-0) control plants. The overall results extend our understanding of the properties and potential functions of LMW 'mammalian-type' PSI plant PAPs.

Materials and methods

Plant material and growth conditions

Heterotrophic Arabidopsis (*Arabidopsis thaliana*, cv. Landsberg erecta) suspension cells were cultured at 21 °C in the dark in conventional Murashige and Skoog medium (pH 5.7) containing 1.25 mM Pi (Caisson Labs, Smithfield, UT, USA) as previously described (Veljanovski *et al.*, 2006; Tran *et al.*, 2010*b*; Ghahremani *et al.*, 2019*b*). For large-scale –Pi subculture, 100 ml aliquots of 7-day-old Pi-replete (+Pi) (5 mM K_2HPO_4) cultures were used to inoculate 2.6 liter Fernbach flasks containing 400 ml of fresh Murashige and Skoog medium lacking Pi (Caisson Labs). –Pi cells were harvested after 7 d by filtration, frozen in liquid N_2, and stored at –80 °C.

Seeds of a homozygous Arabidopsis mutant (*SALK_085340*) with a T-DNA insertion in the last exon of the *AtPAP17* gene (locus At3g17790) (Wang *et al.*, 2014) were kindly provided by Professor Dong Liu (Tsinghua University). A homozygous *atpap26* mutant (*SALK_152821*) was obtained as previously described (Hurley *et al.*, 2010). For routine plant growth, seeds were sown in a standard soil mixture (Sunshine Aggregate Plus Mix 1; SunGro, Vancouver, Canada) and stratified for 3 d at 4 °C before being moved to a growth cabinet where plants were cultivated at 23 °C (16 h:8 h photoperiod at 100 μmol m^{-2} s^{-1} photosynthetically active radiation) with 70% humidity. Plants were fertilized biweekly by subirrigation with 0.25× Hoagland nutrient solution (pH 6.0). To assess the influence of Pi deprivation, leaf senescence, or salinity stress on soil-grown plants, seedlings were grown for 7 d under continuous illumination (100 μmol m^{-2} s^{-1}) on 0.8% (w/v) 'plant cell culture tested' agar (Millipore-Sigma; catalogue # A7921) containing 0.5× Murashige and Skoog medium (Caisson Labs) and 1% (w/v) sucrose, before being transplanted into a 75–85% sphagnum peat moss/perlite soil mix lacking all soluble nutrients (Sunshine Mix 2, SunGro). Plants were cultivated in the growth cabinet for an additional 21 d and fertilized with 0.25× Hoagland's solution containing either 0 (for Pi deprivation studies) or 2 mM KH_2PO_4 (for all other experiments). Whenever Pi was eliminated, it was replaced by 2 mM K_2SO_4 and 0.5 mM MES.

For growth on agar-solidified nutrient media, seeds were surface-sterilized, stratified, and germinated on agar plates as described above. Germinating seedlings of similar size were transferred to horizontal or vertically oriented 1% (w/v) agar plates containing 0.5× 'Pi-free' Murashige and Skoog medium (Caisson Labs) and 1% (w/v) sucrose, supplemented with either 0 or 1.5 mM KH_2PO_4, and cultivated for 14 d at 23 °C (16 h:8 h photoperiod at 100 μmol m^{-2} s^{-1}). For liquid seedling cultures, 5 mg of seeds was surface-sterilized, stratified, and placed in 250 ml Magenta boxes containing 50 ml of 0.5× 'Pi-free' Murashige and Skoog medium (Caisson Labs) supplemented with 1% (w/v) sucrose and 0.2 mM KH_2PO_4, and cultivated at 23 °C under continuous illumination (100 μmol m^{-2} s^{-1}) on an orbital shaker set at 80 rpm. After 7 d, the seedlings were transferred into 75 ml of fresh media containing either 0 or 1.5 mM KH_2PO_4, or 1.5 mM KH_2PO_4 supplemented with 50 mM NaCl, or 1 mM ATP, and cultured for an additional 7 d. The 14-day-old seedlings were rinsed and blotted dry, whereas seedling culture filtrates containing secreted proteins were passed through 0.45 μm syringe filters and concentrated to 0.5 ml using Amicon Ultra-15 centrifugal filter units (30 kDa MWCO). Harvested tissues and seedling culture filtrates were frozen in liquid N_2 for storage at –80 °C.

Prolonged exposure of Arabidopsis leaves to darkness closely mimics natural senescence (Keech *et al.*, 2010; Robinson *et al.*, 2012*a*). Therefore, once rosette leaves of synchronously grown plants were fully expanded, individual leaves were wrapped with tin foil to induce senescence. Leaves appeared 90–100% yellow ~6 d after the leaves were initially covered. Senescing yellow leaves and non-senescent green leaves (opposite, uncovered leaf) were excised, frozen in liquid N_2, and stored at –80 °C.

Protein extraction

For routine extraction of soluble intracellular proteins, quick-frozen suspension cells or seedlings cultivated in liquid media, or leaves of soil-grown plants were ground to a powder under liquid N_2 using a mortar and pestle containing a small spatula of sand and homogenized (1:2; w/v) in 50 mM sodium acetate (pH 5.6) containing 1.5 mM $MgCl_2$, 1 mM phenylmethylsulfonyl fluoride, 5 mM thiourea, and 1% (w/v) insoluble poly(vinylpolypyrrolidone). Homogenates were centrifuged at 14 000 *g* for 10 min at 4 °C. Supernatants were passed through 0.45 μm syringe filters and designated as the soluble intracellular fraction.

Enzyme activity assays and kinetic studies

All enzyme assays were linear with respect to time and concentration of enzyme assayed. One unit (U) of activity is defined as the amount resulting in the use of 1 μmol min^{-1} of substrate at 23 °C. Apparent V_{max}, K_m, and I_{50}(Pi) values were calculated using the enzyme kinetics feature of Graphpad Prism (version 9.0). All kinetic parameters are the means of at least three independent experiments and are reproducible to within ±10% of the mean value.

Phosphatase assay A

The hydrolysis of phosphoenolpyruvate (PEP) to pyruvate was coupled to the lactate dehydrogenase reaction and assayed at 23 °C by monitoring NADH oxidation at 340 nm using a Spectramax Plus Microplate spectrophotometer (Molecular Devices, Sunnyvale, CA, USA). Optimized assay conditions were 50 mM sodium acetate (pH 5.6), 5 mM PEP, 10 mM $MgCl_2$, 0.2 mM NADH, and 3 U ml^{-1} desalted rabbit muscle lactate dehydrogenase in a final volume of 0.2 ml. All assays were initiated by the addition of enzyme preparation and corrected for any background NADH oxidation by omitting PEP from the reaction mixture.

Phosphatase assay B

For substrates other than PEP, Pi released by the phosphatase reaction was quantified as previously described (Bozzo *et al.*, 2004*a*; Veljanovski *et al.*, 2006). Controls were run for background amounts of Pi present at each substrate concentration tested. To calculate activities, a standard curve over the range of 1–133 nmol Pi was constructed for each set of assays.

Peroxidase assays

A chemiluminescence assay was employed to assess the ability of AtPAP17 to catalyze the peroxidation of luminol (5-amino-2,3 dihydro-1,4-phthalazinedione) (Akimoto *et al.*, 1990; Hayman and Cox, 1994). Chemiluminescence was recorded using a Synergy H1 Microplate Reader (BioTek Instruments, Inc.). Reactions were initiated by the addition of 0.1 ml of 20 mM H_2O_2 to 0.1 ml of 50 mM Bis-Tris propane (pH 9.2) containing 1 mM luminol and various amounts of AtPAP17. Photon emission was continuously monitored for 30 s following H_2O_2 addition, and expressed as relative light units using Gen5 Data Analysis Software (BioTek Instruments, Inc.). In control experiments, various amounts of horseradish peroxidase (HRP) (Millipore-Sigma, catalogue # P8375) or BSA were substituted for AtPAP17. We also tested the capacity of purified AtPAP17, HRP, or clarified extracts of Col-0 and *atpap17* leaves to catalyze the peroxidation of guaiacol in the presence of H_2O_2. Guaiacol PRx activity was determined at 470 nm by monitoring guaiacol's oxidation into tetraguaiacol using the Spectramax Plus Microplate reader. Assay conditions were 50 mM Bis-Tris propane (pH 8.2), containing 10 mM guaiacol and 10 mM H_2O_2. The reaction was initiated by adding 200 µl of the assay mixture to a well of a 96-well microtiter plate that contained a 2.5–20 µl aliquot of purified AtPAP17, HRP, or clarified leaf extract.

Purification of AtPAP17 from cell wall extracts of Pi-starved Arabidopsis suspension cells

AtPAP17 was purified from a CW extract prepared from 1 kg of intact –Pi Arabidopsis suspension cells via butyl Sepharose, Fractogel SO_3^-, concanavalin A, and SOURCE™ 15PHE FPLC as previously described for the low mannose AtPAP26-S1 glycoform (Ghahremani *et al.*, 2019*b*). Pooled peak SOURCE 15PHE fractions corresponding to the final AtPAP17 preparation (Fig. 2A) were concentrated to 300 µl, divided into 25 µl aliquots, frozen in liquid N_2, and stored at –80 °C; its APase activity was stable for at least 3 months when stored frozen.

N-terminal microsequencing and MS

N-terminal microsequencing was performed by automated Edman degradation at the Protein and Peptide Sequencing Facility of the Biotechnology Research Institute (Montreal QC, Canada). Peptide mass fingerprinting by matrix-assisted laser desorption ionization quadrupole time-of flight MS was performed as previously described (Tran *et al.*, 2010*b*). Briefly, the 35 kDa protein-staining polypeptide that eluted with the second peak of APase activity during SOURCE 15PHE FPLC (Fig. 2A) was excised from an SDS–PAGE gel, destained, dehydrated, reduced, and alkylated. Digestion was performed using 10 ng of sequencing grade trypsin. Protein identification was performed by searching against the National Center for Biotechnology (NCBI) non-redundant database using the MASCOT server (https://www.matrixscience.com/server.html). For a positive identification, the identified protein must rank as the top hit, match at least four peptides, cover >20% of the total sequence, and generate a MOWSE score greater than the significant threshold at the $P<0.05$ level (MOWSE score >60).

AtPAP17 antibody production

A synthetic AtPAP17 peptide was designed by aligning the deduced amino acid sequences of the 29 AtPAP isozymes (Li *et al.*, 2002) using Geneious (http://www.geneious.com). A 19 amino acid, N-terminal region unique to AtPAP17 was identified (i.e. VSNGELQRFIEPAKSDGSV). The synthetic peptide (Lifetein LLC, Somerset, NJ, USA) was conjugated to keyhole limpet hemocyanin (Imject™ Maleimide Activated mcKLH; Thermo Scientific™, Cat. #77605) and emulsified in Titer Max Gold adjuvant (Uptima, Interchim Research, Cedex, France) according to the manufacturer's instructions. The conjugated synthetic peptide (1 mg) was injected subcutaneously into a New Zealand rabbit. A secondary injection (0.5 mg) was administered after 28 d. One week following the final injection, blood was collected by cardiac puncture and the anti-AtPAP17 immune serum was frozen in liquid N_2 and stored at -80 °C.

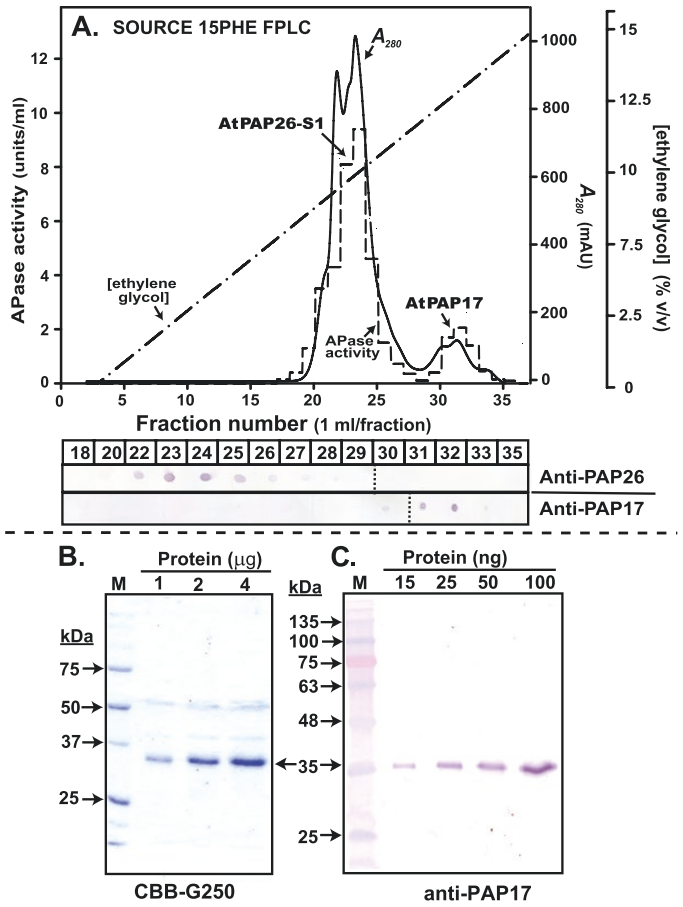

Fig. 2. Purification of AtPAP17 from a CW extract of Pi-deprived Arabidopsis suspension cells. (A) SOURCE 15PHE hydrophobic interaction FPLC of pooled concanavalin A–Sepharose 'flow through' fractions containing the low mannose AtPAP26-S1 glycoform resolved two peaks of APase activity, with the first representing AtPAP26-S1 (Ghahremani *et al.*, 2019*b*). A 2 µl aliquot of each APase activity-containing fraction was subjected to immunodot blotting with anti-PAP26 or anti-PAP17 as indicated. (B, C) SDS–PAGE of indicated amounts of pooled fractions corresponding to the second APase activity peak shown in (A) was followed by protein staining using Coomassie Blue G-250 (CBB-G250) (B) or immunoblotting with anti-PAP17 (C). 'M' indicates various non-pre-stained (B) or pre-stained (C) molecular mass standards.

Protein electrophoresis, immunoblotting, and in-gel APase activity staining

SDS–PAGE, subunit molecular mass estimation via SDS–PAGE, immunoblotting onto poly(vinylidene) difluoride membranes, and visualization of immunoreactive polypeptides using an alkaline phosphatase-tagged secondary antibody and chromogenic detection were conducted as previously described (Veljanovski *et al.*, 2006). Non-denaturing PAGE was performed using Bio-Rad Mini-Protean TGX gels (10% acrylamide), a running buffer composed of 0.1 M Tris and 0.15 M glycine (pH 6.8), and a sample loading buffer consisting of 62.5 mM Tris–HCl (pH 6.8) containing 25% (v/v) glycerol. Following electrophoresis, gels were incubated for 20 min in 100 mM

Na-acetate (pH 5.3) containing 10 mM $MgCl_2$. Red APase activity-staining bands were visualized by placing gels in the same buffer containing 1% (w/v) Fast Garnet GBC salt and 0.03% (w/v) β-naphthyl-P. All SDS– and non-denaturing PAGE gels, and immunoblots were replicated a minimum of three times, with representative results shown in the various figures.

Determination of protein, chlorophyll, total P, and anthocyanin concentrations

Protein concentrations were determined using a modified Bradford assay with bovine γ-globulin as the standard (Bozzo *et al.*, 2002). Chlorophyll, total P, and anthocyanin contents were determined as previously described (Hurley *et al.*, 2010; Robinson *et al.*, 2012*a*; Knowles and Plaxton, 2013).

RNA extraction and quantitative real-time PCR analysis

Total RNA was extracted from 21-day-old +Pi and –Pi Col-0, *atpap17*, and *atpap26* seedlings using TRIzol Reagent (Thermo Fisher Scientific) according to a published protocol (Rio *et al.*, 2010) with minor changes to the RNA precipitation steps. Briefly, total RNA was precipitated with isopropanol–sodium acetate and then re-precipitated with lithium chloride to remove genomic DNA (gDNA). For cDNA synthesis, 200 ng of RNA was reverse transcribed by the SuperScript III First-Strand Synthesis System (Thermo Fisher Scientific) according to the manufacturer's instructions. Quantitative real-time PCR (qRT-PCR) was performed using PerfeCTa SYBR Green FastMix (QuantaBio) in a StepOnePlus RT-PCR system (Thermo Fisher Scientific) with gene-specific primers (Supplementary Table S1). Relative *AtPAP17* and *AtPAP26* expression was calculated by normalizing the C_T value to that of the reference genes *TIP41* and *ACTIN* (Yang *et al.*, 2015).

Subcellular localization of AtPAP17–GFP fusion protein

An *AtPAP17* cDNA was obtained from the Arabidopsis Biological Resource Center (clone U23382) and amplified using PCR and appropriate primers (Supplementary Table S1). The resulting PCR fragment, containing the entire ORF of *AtPAP17*, was digested with *Kpn*I–*Xba*I and ligated into similarly digested *pMDC84-GFP* (Curtis and Grossniklaus, 2003), yielding *pMDC84-AtPAP17-GFP*. *pSAT4A-AtPAP26-mCherry* was obtained as previously described (Hurley *et al.*, 2010). Culturing of Arabidopsis (cv. Landsberg erecta) suspension cells in liquid medium (Murashige and Skoog, 1962), and co-transient transformations of cells (4 d post-subculturing) with 5 mg of each plasmid using biolistic bombardment were performed as previously described (Hurley *et al.*, 2010). Bombarded cells were incubated for 8 h to allow expression and sorting of the expressed proteins, and then fixed in 8% (w/v) formaldehyde. Images were acquired using a Zeiss Axioscope 2 MOT epifluorescence microscope with a ×63 plan apochromat oil-immersion objective (Carl Zeiss Inc.). Image capture was performed using a Retiga 1300 charge-coupled device camera (Qimaging) and Northern Eclipse 5.0 software (Empix Imaging Inc.). Figure compositions were generated using Adobe Photoshop CS (Adobe Systems Inc.). Fluorescence images of cells shown are representative of at least three separate experiments (i.e. bombardments), whereby >25 transformed cells were analyzed.

Statistical analysis

Unless otherwise stated, all statistical analyses were performed using one-way ANOVA. Differences were considered significant at $P<0.05$.

Results

Purification of AtPAP17 from cell walls of Pi-deprived Arabidopsis suspension cells

Ghahremani *et al.* (2019*a*) isolated a pair of secreted AtPAP26 glycoforms (AtPAP26-S1 and -S2) from the CW proteome of –Pi Arabidopsis suspension cells. During lectin affinity chromatography on concanavalin A–Sepharose, the low mannose AtPAP26-S1 failed to bind, whereas the high mannose AtPAP26-S2 was bound and then eluted using a mannopyranoside gradient (Ghahremani *et al.*, 2019*a*). SOURCE 15PHE hydrophobic interaction FPLC of the pooled non-binding concanavalin A fractions unexpectedly resolved two peaks of APase activity, with the first, larger peak representing AtPAP26-S1 (Fig. 2A) (Ghahremani *et al.*, 2019*a*). Fractions corresponding to the second APase activity peak shown in Fig. 2A (specific activity=27.5 U mg^{-1}) were pooled and concentrated for further investigation. The major 35 kDa protein-staining polypeptide observed following SDS–PAGE of this preparation (Fig. 2B) was subjected to N-terminal microsequencing, as well as peptide mass fingerprinting using MS. Comparison with database sequences identified it as AtPAP17 (At3g17790), with 51% sequence coverage obtained during MS analysis (Fig. 3; Supplementary Table S2). These results indicate that AtPAP17 is localized to the CW of the –Pi cells.

Bioinformatic analysis

AtPAP17 shares 56–59% sequence identity with its Group IIIb AtPAP paralogs, which include AtPAP3, AtPAP4, AtPAP7, and AtPAP8 (Fig. 3; Supplementary Fig. S1), whereas its identity with its closest orthologs from other plant species is >88% (Supplementary Table S3). *In silico* analysis of AtPAP17's cDNA deduced amino acid sequence revealed that it is translated as a 338 amino acid polypeptide with a predicted molecular mass of 38.3 kDa (Fig. 3). The 3.3 kDa discrepancy with the 35 kDa molecular mass of purified AtPAP17 as estimated by SDS–PAGE (Fig. 2B) can be explained by cleavage of a signal peptide. Signal P (http://www.cbs.dtu.dk/services/SignalP/) predicted that AtPAP17's N-terminus contains a 31 amino acid signal peptide that targets it to the secretory pathway, which includes secreted and vacuolar proteins. The N-terminal sequence of AtPAP17 isolated from the CW (Fig. 3) or intracellular (del Pozo *et al.*, 1999) fraction of –Pi Arabidopsis begins at position 32, confirming an actual signal peptide length of 31 amino acids.

Glycosylation is an important post-translational modification that can modulate enzymatic stability, localization, and kinetic properties. Although all characterized PAPs are glycosylated, few details of their *N*-linked glycans are available (Olczak and Olczak, 2007; Del Vecchio *et al.*, 2014; Ghahremani *et al.*, 2016, 2019*b*). AtPAP17 is predicted to have a single *N*-linked glycosylation site at Asn61, which forms part of a conserved NX(S/T) glycosylation motif (where X is any amino acid except Pro) (Fig. 3). AtPAP17 glycosylation at Asn61 was confirmed during an *N*-glycopeptide profiling study of the Arabidopsis inflorescence proteome, which employed wheat germ lectin affinity chromatography to enrich glycopeptides (Xu *et al.*, 2016).

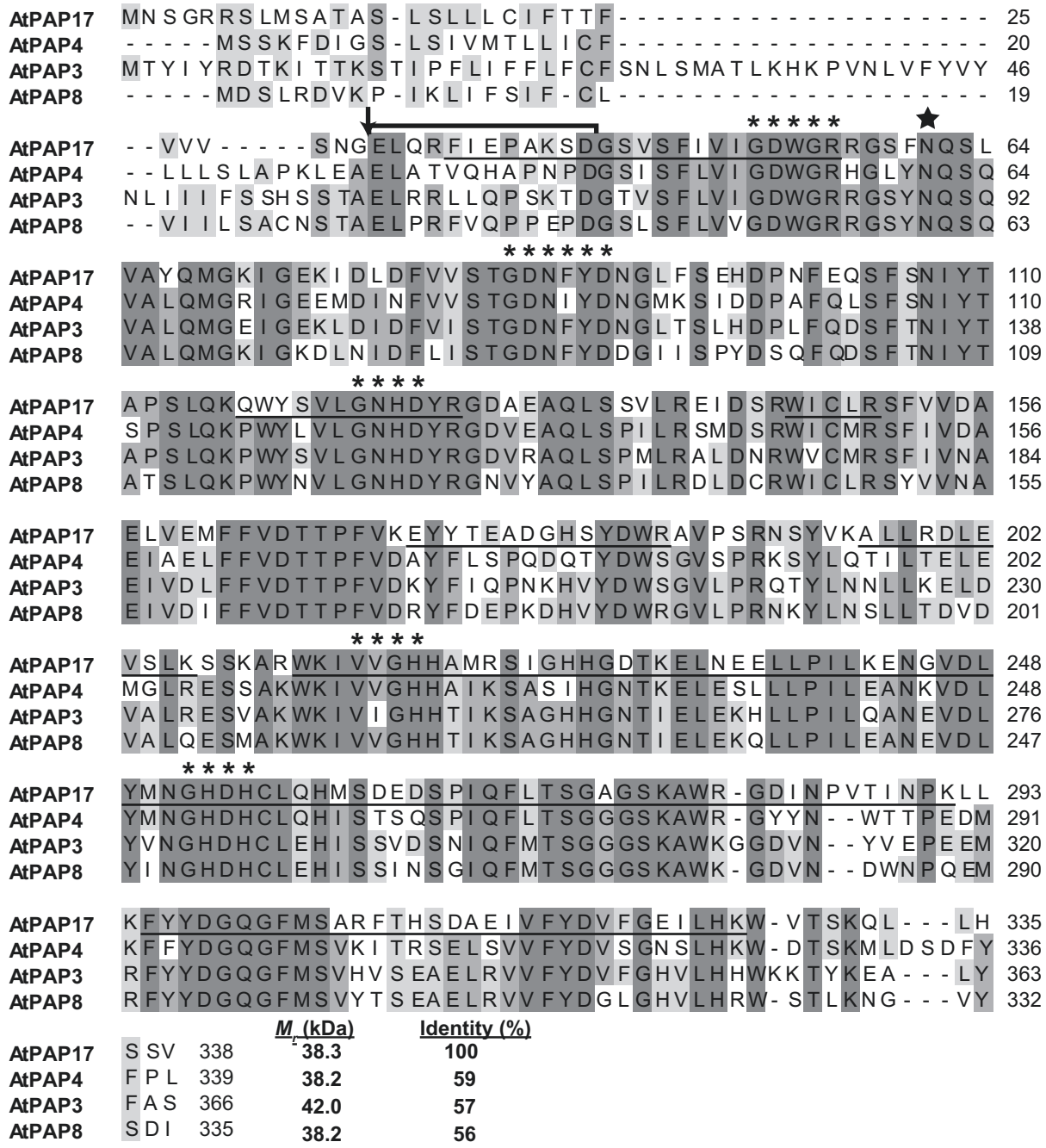

Fig. 3. Deduced amino acid sequence alignment of AtPAP17 (At3g17790) with other Group IIIb members of the Arabidopsis PAP family. These are AtPAP3 (At1g14700), AtPAP4 (At1g25230), and AtPAP8 (At2g01890) (Supplementary Fig. S1). Tryptic peptides derived from the 35 kDa protein-staining polypeptide of purified AtPAP17 (Fig. 1B) were subjected to peptide mass fingerprinting using MALDI-TOF MS, and are underlined. The arrow indicates the predicted signal peptide cleavage site, whereas the N-terminal sequence determined for purified AtPAP17 is overlined. The star indicates the glycosylation site for AtPAP17 (Asn61) and its three paralogs. Conserved PAP sequence motifs containing metal-ligating residues are marked with asterisks. Identical and similar amino acids are denoted by dark and light gray shading, respectively.

AtPAP17 is dual-localized to the extracellular matrix and lytic vacuoles of Pi-deprived Arabidopsis

In contrast to the current study, del Pozo *et al.* (1999) purified AtPAP17 from the soluble, intracellular fraction of –Pi Arabidopsis seedlings. To further evaluate AtPAP17's subcellular localization, a protocol was devised for simultaneous extraction of intracellular and ionically bound CW proteomes from –Pi Arabidopsis cell cultures that exhibit negligible contamination by CW and cytoplasmic marker proteins, respectively (Supplementary Fig. S2). Immunoblotting demonstrated that

the abundant cytosolic marker enzymes aldolase and sucrose synthase were undetectable in the CW extract (Supplementary Fig. S3A, B). In contrast, immunoreactive 40 kDa aldolase and 93 kDa sucrose synthase polypeptides that co-migrated with the respective purified enzymes were readily detected on parallel immunoblots of the corresponding intracellular fraction (Supplementary Fig. S3A, B). The same extracts were subjected to immunoblotting for AtPAP25, a 55 kDa HMW AtPAP (Supplementary Fig. S1) previously purified and characterized from the CW proteome of the –Pi Arabidopsis cells (Del Vecchio *et al.*, 2014). A 55 kDa immunoreactive polypeptide that co-migrated with purified AtPAP25 was detected on an anti-(AtPAP25) immunoblot of the CW extract, but not the corresponding intracellular extract (Supplementary Fig. S3C). SDS–PAGE followed by multiplex phosphoprotein and total protein staining with Phos-tag and SYPRO-Red fluorescent stains, respectively, revealed that the CW and intracellular samples exhibited highly dissimilar banding patterns (Supplementary Fig. S3D). Results shown in Supplementary Fig. S3 indicate that the protocol outlined in Supplementary Fig. S2 is reliable for the concurrent isolation of soluble intracellular and ionically bound CW proteomes from the Arabidopsis cells.

Non-denaturing PAGE followed by in-gel APase activity staining allows visualization of the presence and relative abundance of HMW and LMW APase isozymes present in plant extracts (Hurley *et al.*, 2010; Tran *et al.*, 2010*b*; Robinson *et al.*, 2012*a*; Wang *et al.*, 2014; Sun *et al.*, 2018; Wang and Liu, 2018). Non-denaturing PAGE of CW and intracellular extracts from the –Pi suspension cells revealed a LMW APase activity-staining band that co-migrated with purified AtPAP17, and that was well resolved from other co-extracted APases (Fig. 4A). AtVSP3, a 29 kDa PSI vegetative storage protein that exhibits APase activity (Sun *et al.*, 2018), was only detected in the intracellular fraction of the –Pi suspension cells and, like AtPAP17, showed marked turnover 48 h following resupply of 2 mM Pi to the –Pi cells (Fig. 4A). Sun *et al.* (2018) purified and characterized native AtVSP3 from the soluble, intracellular fraction of hydroponically cultivated –Pi Arabidopsis seedlings.

Comparable results were obtained following non-denaturing PAGE of intracellular and secretome samples of hydroponic cultures of 2-week-old Arabidopsis seedlings that had been cultivated in –Pi liquid media for 7 d prior to harvest (Fig. 4B). The LMW APase activity-staining band of the –Pi samples that co-migrated with purified AtPAP17 was absent in corresponding extracts of +Pi plants, as well as a –Pi *atpap17* T-DNA mutant that is discussed below. In contrast to the suspension cells, the fastest migrating APase activity-staining band representing AtVSP3 (Sun *et al.*, 2018) was detected in intracellular and secretome fractions of the Arabidopsis seedlings (Fig. 4A, B).

To visualize subcellular AtPAP17 localization in intact cells, its coding region was fused with a *GFP* (green fluorescent protein) reporter gene and transiently expressed in the Arabidopsis suspension cells. Epifluorescence microscopy demonstrated that AtPAP17–GFP localized to lytic vacuoles (Fig. 5A), as evidenced by its co-localization with co-expressed AtPAP26–mCherry (Fig. 5B, C), serving as a well-characterized vacuole marker fusion protein (Hurley *et al.*, 2010; Ghahremani *et al.*, 2019*a*). This result is consistent with those of Fig. 4, as well as of del Pozo *et al.* (1999) who isolated AtPAP17 from the intracellular fraction of –Pi Arabidopsis seedlings.

Pi deprivation, leaf senescence, and salinity stress induce AtPAP17 gene and protein expression

Transcript profiling via semi-quantitative RT-PCR and/or qRT-PCR corroborated many reports (see, for example, del Pozo *et al.*, 1999; Müller *et al.*, 2004; Veljanovski *et al.*, 2006; Tran and Plaxton, 2008; Hurley *et al.*, 2010) that *AtPAP17* expression is strongly induced in –Pi suspension cells, and shoots and roots of –Pi seedlings (Supplementary Fig. S4). Similarly, the non-denaturing PAGE results shown in Fig. 4 indicated that AtPAP17 was *de novo* synthesized by the –Pi suspension cells and seedlings. Interestingly, intracellular and secreted AtPAP17 polypeptides appeared to be largely turned over within 48 h of resupply of 2 mM Pi to the –Pi suspension cells (Fig. 4A).

While the PSR involves strategies such as the up-regulation of secreted and vacuolar PAPs and nucleases to improve Pi acquisition and use efficiency, the redistribution of Pi from the Po pool (particularly rRNA) of senescing leaves to developing seeds and immature leaves makes a crucial contribution to plant Pi use efficiency (Stigter and Plaxton, 2015). *AtPAP17* transcript profiling and *AtPAP17* promoter–β-glucuronidase (GUS) reporter gene fusion assays demonstrated that *AtPAP17* transcription is strongly induced during leaf senescence, as well as in roots and shoots during salinity stress (del Pozo *et al.*, 1999; Robinson *et al.*, 2012*a*). This was paralleled by *de novo* synthesis of 35 kDa AtPAP17 polypeptides as indicated by non-denaturing PAGE and in-gel phosphatase activity staining of extracts prepared from senescing Arabidopsis leaves, or intracellular extracts and culture filtrates of hydroponically cultivated +Pi seedlings that had been incubated with 50 mM NaCl for 7 d prior to harvest (Fig. 6A, B). The LMW phosphatase activity-staining band of the various samples that co-migrated with purified AtPAP17 was absent following non-denaturing PAGE of corresponding extracts of the *atpap17* T-DNA mutant.

Interrogation of mRNA expression datasets for the AtPAP family deposited in the Bio-analytic Resource for Plant Biology (http://bar.utoronto.ca) confirmed that: (i) *AtPAP17* is markedly induced in shoots and roots by multiple abiotic stresses, particularly during Pi deprivation, and osmotic and salt stress; and (ii) the stress-inducible expression patterns of *AtPAP17* appear to be relatively unique compared with other AtPAP family members, including its closest LMW paralogs AtPAP3, AtPAP4, AtPAP7, and AtPAP8 (Supplementary Fig. S5). While *AtPAP17* transcription is induced by multiple stresses, it is not a general stress response gene since its expression was unresponsive to nitrogen or potassium starvation, or oxidative stress mediated by paraquat or salicylic acid (del Pozo *et al.*, 1999).

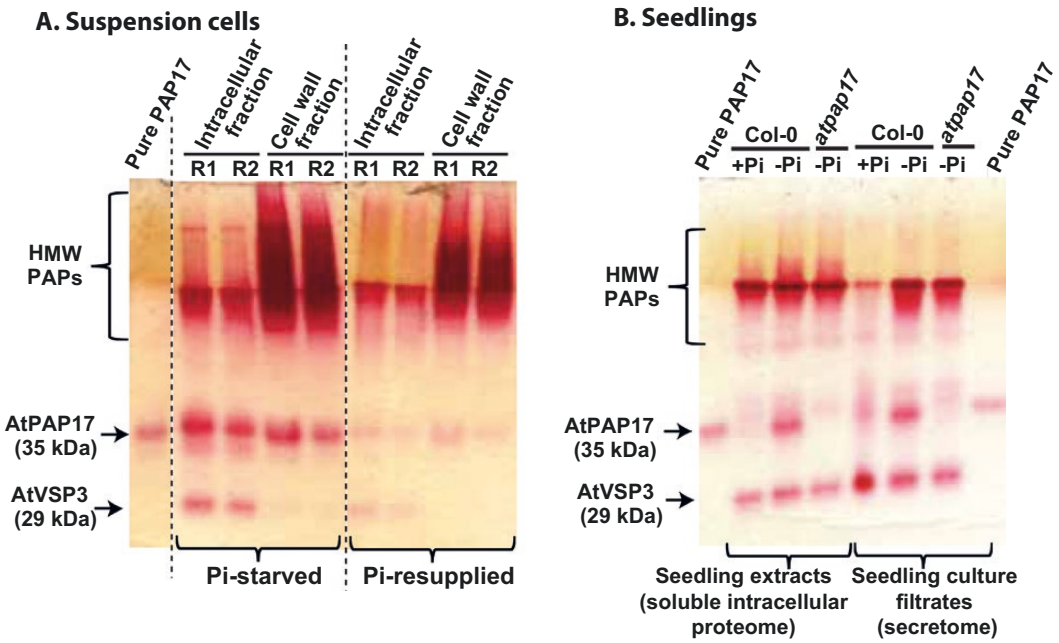

Fig. 4. AtPAP17 is up-regulated and dual-localized to the intracellular fraction and extracellular matrix of Pi-deprived Arabidopsis cell cultures and seedlings. (A) Non-denaturing PAGE was followed by in-gel APase activity staining of purified AtPAP17 (150 ng), alongside intracellular and CW extracts of –Pi suspension cells, as well as –Pi cells that had been resupplied with 2 mM NaPi for 48 h (designated as 'Pi-resupplied') as described by Mehta *et al.* (2021). Intracellular and CW extracts were prepared according to the protocol outlined in Supplementary Fig. S3. About 10 μg and 5 μg of protein from replicate intracellular and CW extracts (R1 and R2) was loaded per lane, respectively. (B) Non-denaturing PAGE was followed by in-gel APase activity staining of purified AtPAP17 (150 ng), alongside clarified extracts and corresponding concentrated growth media (12 μg per lane) of 14-day-old wild-type (Col-0) and homozygous *atpap17* T-DNA insertional mutant seedlings (*atpap17*) (Wang *et al.*, 2014) that had been hydroponically cultivated for the previous 7 d in media containing 1.5 mM or 0 mM KPi (+Pi and –Pi, respectively). Prior to analysis, growth medium containing secreted proteins was filtered and concentrated ~100-fold as described in the Materials and methods. (A and B) 'HMW PAPs' include the 100 kDa AtPAP26 homodimer which dual-localizes to the cell vacuole and extracellular matrix of –Pi Arabidopsis (Veljanovski *et al.*, 2006; Hurley *et al.*, 2010; Tran *et al.*, 2010*b*; Robinson *et al.*, 2012*b*; Shane *et al.*, 2014; Wang *et al.*, 2014), whereas the fastest mobility APase activity staining band is due to AtVSP3, a 29 kDa Pi starvation-inducible vegetative storage protein that exhibits APase activity (Sun *et al.*, 2018). The gels were stained for phosphatase activity using β-naphthyl-phosphate and Fast Garnet GBC.

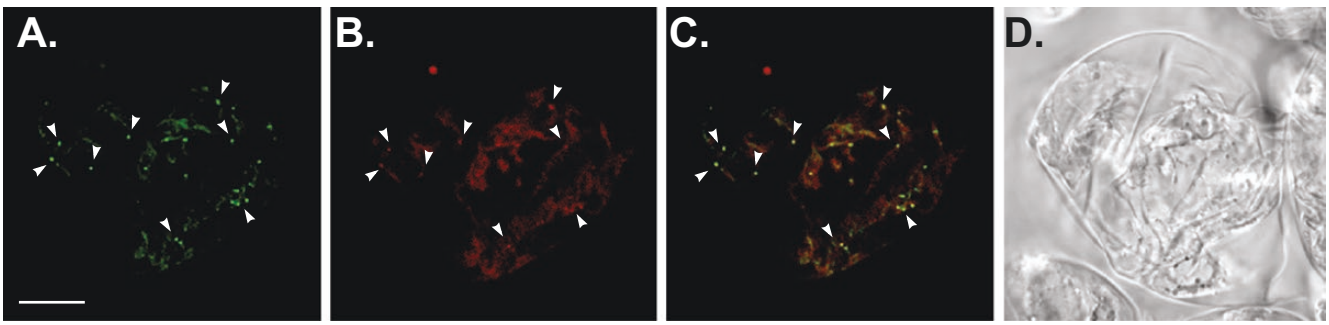

Fig. 5. AtPAP17–GFP localizes to lytic vacuoles of transiently transformed Arabidopsis suspension cells. Heterotrophic Arabidopsis suspension cells were co-transformed via biolistic bombardment with AtPAP17–GFP and AtPAP26–mCherry, the latter serving as a well-characterized lytic vacuole marker (Hurley *et al.*, 2010; Ghahremani *et al.*, 2019*a*). Following bombardment, cells were incubated for 8 h to allow for gene expression and protein sorting, then fixed in formaldehyde and viewed using epifluorescence microscopy. Note that the fluorescence patterns attributable to AtPAP17–GFP (A) and AtPAP26–mCherry (B) co-localize, as evidenced by the yellow color in the merged image (C); obvious examples of co-localization are also indicated by arrowheads. (D) The differential interference contrast image is also shown. Scale bar=10 μm.

AtPAP17 immunological and physical properties

For production of anti-AtPAP17 antibodies (anti-PAP17), a 19 amino acid peptide matching a portion of AtPAP17's N-terminus was synthesized with an N-terminal cysteine residue to enable its conjugation to keyhole limpet hemocyanin prior to rabbit immunization. A 1:500 dilution of the immune serum cross-reacted with as little as 15 ng of purified AtPAP17 (Fig. 2C). AtPAP17 is immunologically distinct from AtPAP12, AtPAP25, or AtPAP26 (Supplementary Fig. S6), which corroborates its distant phylogenetic relationship with these HMW

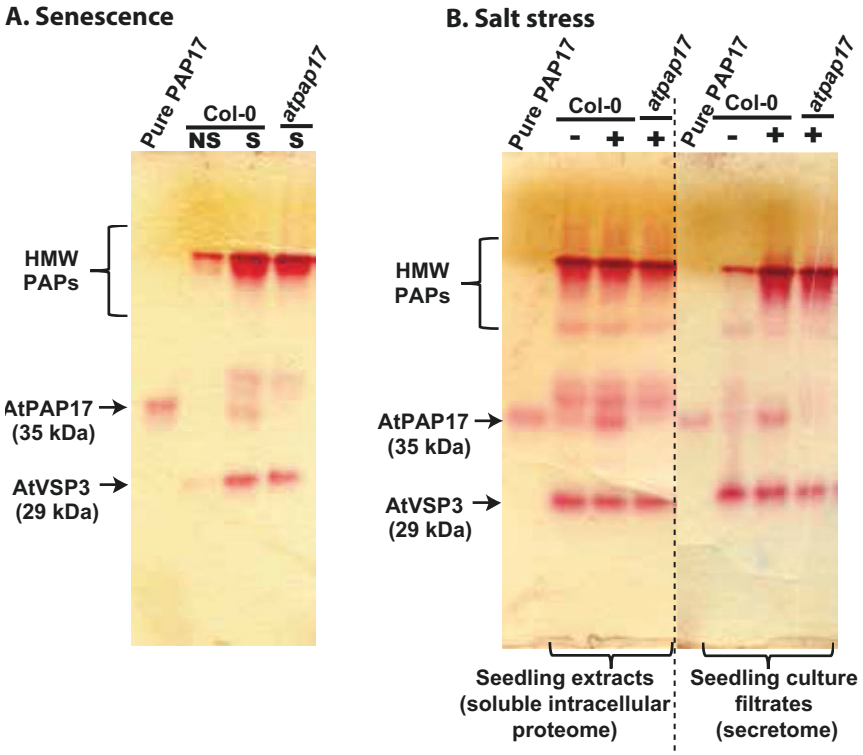

Fig. 6. AtPAP17 is up-regulated during leaf senescence or following salinity stress. Non-denaturing PAGE was followed by in-gel APase activity staining of purified AtPAP17 (150 ng), alongside: (A) clarified extracts (15 µg protein per lane) of non-senescing (NS) versus senescing (S) leaves of 21-day-old wild-type (Col-0) and *atpap17* mutant seedlings (Wang *et al.*, 2014) that had been cultivated in a standard soil mix under a regular light/dark regime, and (B) clarified extracts and corresponding concentrated growth medium (8 µg per lane) of 14-day-old wild-type (WT) and *atpap17* mutant plants that had been hydroponically cultivated for the previous 7 d in +Pi media containing 0 (–) or 50 mM NaCl (+). Prior to analysis, growth medium containing secreted proteins was filtered and concentrated as described in the Materials and methods.

group Ia members of the AtPAP family (Supplementary Fig. S1). Despite its sensitivity (Fig. 2C), the anti-AtPAP17 failed to detect any immunoreactive polypeptides following immunoblotting of clarified extracts prepared from –Pi suspension cells or seedlings, using either chromogenic or enhanced chemiluminescent detection. This suggests that cellular levels of AtPAP17 polypeptides are comparatively low relative to highly expressed PAPs such as AtPAP26 (Veljanovski *et al.*, 2006; Tran *et al.*, 2010*b*; Robinson *et al.*, 2012*a*).

When an aliquot of the final AtPAP17 preparation was subjected to gel filtration on a calibrated Superdex 75 column and analyzed by SDS–PAGE, a single 35 kDa protein-staining polypeptide was observed that cross-reacted with anti-AtPAP17 (Supplementary Fig. S7A), indicating that AtPAP17 had been purified to apparent homogeneity. AtPAP17's native molecular mass was estimated by analytical gel filtration to be 35±4 kDa (mean ±SE of n=3 determinations) (Supplementary Fig. S7B). Thus, native AtPAP17 exists as a 35 kDa monomer, as reported for PvPAP3 and HsACP5, LMW PAP orthologs of common bean and humans, respectively (Liang *et al.*, 2010; Schenk *et al.*, 2013).

AtPAP17 was relatively heat stable, losing no APase activity when 10 µl aliquots containing 0.5 µg of the purified enzyme were incubated for 4 min at 50 °C or 60 °C. However, a 90% loss in APase activity that was detected following its 4 min incubation at 70 °C indicates that AtPAP17 undergoes irreversible denaturation beyond 60 °C. Similar results were obtained with PvPAP3, a 34 kDa PSI and secreted AtPAP17 ortholog of common bean (Liang *et al.*, 2010).

AtPAP17 phosphatase kinetic properties

Unless otherwise indicated, all kinetic studies were performed using phosphatase assay A. Purified AtPAP17 was activated ~50% by 10 mM $MgCl_2$ at pH 5.6. Similar results were reported for a variety of plant PAPs, including the LMW PvPAP3 (Liang *et al.*, 2010). Thus, 10 mM $MgCl_2$ was routinely included in AtPAP17's phosphatase assay mixture. AtPAP17 displayed a broad pH APase activity profile, exhibiting maximal activity between pH 5.5 and 7.5 (Fig. 7A).

Substrate specificity

APase activity of AtPAP17 was determined at pH 5.6 using phosphatase assay B and a wide range of phosphorylated compounds tested at a concentration of 5 mM. Similar to most PAPs characterized to date (Tran *et al.*, 2010*a*), AtPAP17 exhibited broad substrate specificity (Tables 1, 2). PEP, phenyl-P,

para-nitrophenyl-P, α- and β-naphthyl-P, and ATP were the most effective substrates (Table 1). AtPAP17 also showed phosphatase activity with phosphotyrosine, phosphothreonine, and phosphoserine, as well as the egg storage phosphoprotein phosvitin (Table 2). However, no phosphodiesterase activity was detected with 5 mM bis-*para*-nitrophenyl-P. AtPAP17 also failed to use 5 mM phytate as a substrate, which demonstrates that in contrast to AtPAP15 (Tran *et al.*, 2010*a*; Feder *et al.*, 2020), it is not a phytase. Sequence alignment revealed that AtPAP17 lacks a critical 'RKEA' motif that is believed to confer phytase activity to PAPs such as AtPAP15 (Supplementary Fig. S8) (Feder *et al.*, 2020).

Kinetic parameters of AtPAP17 for those P-esters that were the most effective substrates were determined at pH 5.6 (Table 2). AtPAP17's catalytic efficiency (V_{max}/K_m) with PEP was at least 7-fold greater than that of any of other substrate. Hyperbolic saturation kinetics were routinely observed, with a low K_m(PEP) value of 100 μM in the same range as that reported for AtPAP12, AtPAP25, or AtPAP26 purified from CW extracts of the –Pi cells (Tran *et al.*, 2010*b*; Del Vecchio *et al.*, 2014; Ghahremani *et al.*, 2019*a*). However, AtPAP17's V_{max}(pNPP) value of ~20 U mg^{-1} (Table 2) was far lower than the specific pNPP hydrolyzing activity of 1333 U mg^{-1} reported by del Pozo *et al.* (1999) for AtPAP17 purified from –Pi Arabidopsis seedlings. The reason for this discrepancy is unknown, but a maximal pNPP hydrolyzing activity in the range of 20 U mg^{-1} was consistently achieved for multiple AtPAP17 preparations that we purified from the –Pi cells. AtPAP17's K_m(pNPP) value of 0.85 mM (Table 2) was comparable with the value of 0.4 mM reported for its LMW ortholog isolated from rat bones (Ek-Rylander *et al.*, 1997).

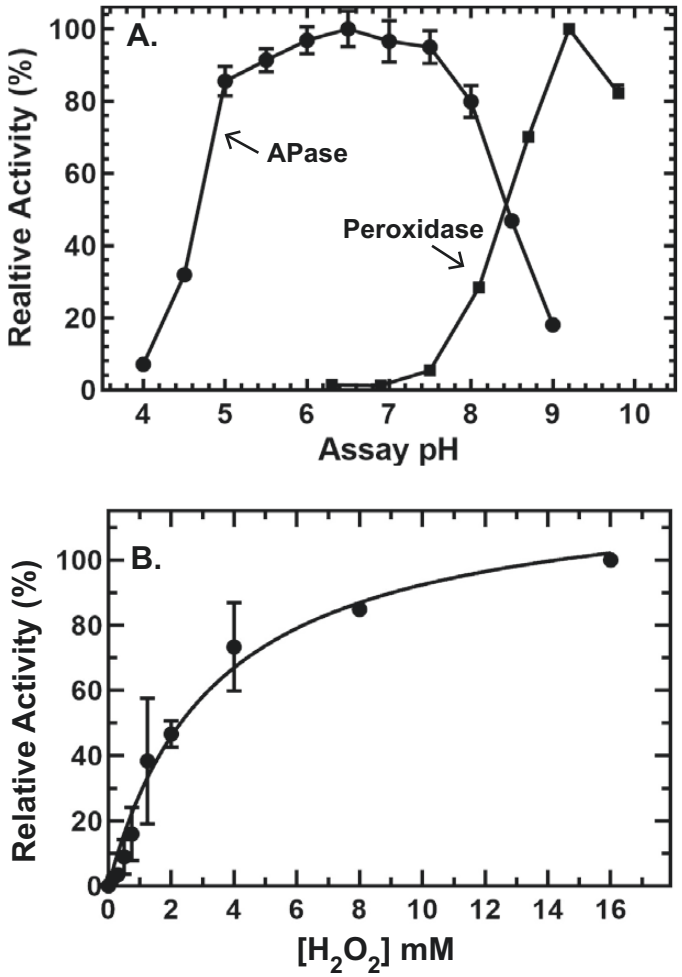

Fig. 7. (A) The phosphatase versus PRx activity of AtPAP17 as a function of assay pH, and (B) relationship between its PRx activity and H_2O_2 concentration. Assays were buffered by: (A) a mixture of 25 mM sodium acetate, 25 mM MES, and 25 mM Bis-Tris propane, and (B) 50 mM Bis-Tris-propane (pH 9.2). All values in (A) and (B) represent the mean ±SE of *n*=4 separate determinations; where not visible, the error bars are too small to be seen.

Metabolite and ion effects

Several compounds were examined for effects on AtPAP17's APase activity at pH 5.6 with 5 mM PEP as substrate (Supplementary Table S4). Tartrate (5 mM) exerted no influence on AtPAP17 activity, which is consistent with its PAP classification (Schenk *et al.*, 2013). In contrast, potent inhibition was exerted by molybdate, vanadate, and Zn^{2+}, as reported for other PAPs (Bozzo *et al.*, 2004*a*; Veljanovski *et al.*, 2006; Tran *et al.*, 2010*a*, *b*; Del Vecchio *et al.*, 2014). AtPAP17

Table 1. Substrate specificity of purified AtPAP17

Substrate	Relative activity
PEP	100
Phenyl-P	73
para-nitrophenyl-P	70
β-Naphthyl-P	56
α-Naphthyl P	40
ATP	39
Phosphotyrosine	35
6-Phosphogluconate	35
β-Glycerophosphate	35
ADP	31
Glucose-6-P	30
Phosphothreonine	28
Glycerate-3-P	23
Fructose-6-P	15
Phosphoserine	11
Glucose-1-P	8
AMP	8
DeoxyAMP	7
Phosvitin	2

APase activity was determined at pH 5.6 with 5 mM of each compound (or 10 mg ml^{-1} phosvitin, an egg storage phosphoprotein) using phosphatase assay B as described in the Materials and methods. APase activity is expressed relative to the rate of Pi hydrolysis from PEP set at 100%. All values are the means of at least three independent determinations and are reproducible within ±10% of the mean.

Table 2. Substrate saturation kinetics of AtPAP17

Substrate	V_{max}(U mg^{-1})	K_m(mM)	V_{max}/K_m(U mg^{-1} mM^{-1})
PEP	30	0.1	300
Phenyl-P	22	0.5	44
p-Nitrophenyl-P	21	0.85	25
β-Naphthyl-P	17	1.2	14
α-Naphthyl-P	12	1.6	7.5

Kinetic parameters were determined at pH 5.6. All values are the means of at least three independent determinations and are reproducible within ±10% of the mean.

also exhibited effective feedback inhibition by Pi as reflected by its relatively low I_{50}(Pi) value of 0.93±0.10 mM. Coupled with the rapid repression of *AtPAP17* transcription, and turnover of AtPAP17 polypeptides following Pi resupply to –Pi Arabidopsis (Fig. 4A) (del Pozo *et al.*, 1999; Müller *et al.*, 2004; Veljanovski *et al.*, 2006; Mehta *et al.*, 2021), this indicates tight feedback control by Pi that would curtail AtPAP17's phosphatase activity except when cellular Pi levels are relatively low.

AtPAP17 peroxidase activity

Several mammalian and plant PAPs, including HsACP5, AtPAP17, and AtPAP26, were characterized as bifunctional enzymes that exhibit APase and PRx activities (del Pozo *et al.*, 1999; Hayman and Cox, 1994; Bozzo *et al.*, 2002, 2004*a*; Veljanovski *et al.*, 2006). We initially attempted to measure AtPAP17's PRx activity using a spectrophotometric assay based upon H_2O_2-mediated oxidation of guaiacol (2-methoxyphenol) to tetraguaiacol (biphenoquinone). Although this assay readily detected PRx activity in control HRP assays, as well as in pooled fractions from earlier steps of AtPAP17 purification, it failed to detect any activity during parallel assays with up to 2.5 μg of our final AtPAP17 preparation. We next investigated the ability of AtPAP17 to catalyze the peroxidation of luminol in the presence of H_2O_2 using a chemiluminescence assay. The limitations imposed by the requirements of the luminol reaction negate chemiluminescence determinations at acidic pH values. However, in the pH range 7–10, the peroxidative activity of AtPAP17 elicited significant chemiluminescence relative to equimolar concentrations of BSA (Supplementary Fig. S9A), with maximal activity occurring at about pH 9.2 (Fig. 7A). The induction of chemiluminescence probably resulted from formation of hydroxyl radicals as products of the Fenton reaction (Fig. 1) (Schenk *et al.*, 2013). Photon emission generated by the PRx activity of AtPAP17 was proportional to the protein concentration (Supplementary Fig. S9A). Calibration of the luminometer with known amounts of HRP (3236 U mg^{-1}) (Supplementary Fig. S9B) allowed us to estimate a specific PRx activity of 41 U mg^{-1} for our final AtPAP17 preparation when assayed at pH 9.2 with 10 mM H_2O_2 and 1 mM luminol. AtPAP17's H_2O_2 saturation kinetics were examined at pH 9.2 and revealed standard Michaelis–Menten kinetics (Fig. 7B) with a relatively high $K_m(H_2O_2)$ value of 3.4±0.7 mM, compared with glutathione or ascorbate PRxs, and HRP that all exhibit $K_m(H_2O_2)$ values in the micromolar range (Akimoto *et al.*, 1990).

Impact of AtPAP17 loss of function during Pi deprivation, leaf senescence, and salinity stress

Wang *et al.* (2014) capitalized on the publicly available T-DNA insertion lines of Arabidopsis to identify and isolate a homozygous *atpap17* mutant (SALK_085340) that contains a T-DNA insert in its last exon (Supplementary Fig. S10A). We confirmed this by extracting gDNA from leaves of *atpap17* and Col-0 plants followed by PCR screening using gene-specific and T-DNA left border primers (Supplementary Fig. S10B; Supplementay Table S1). SALK_085340 is a null allele, as demonstrated by the absence of *AtPAP17* mRNA in –Pi *atpap17* plants (Wang *et al.*, 2014). The non-denaturing PAGE results of Figs 4 and 6 established that: (i) up-regulation of AtPAP17's phosphatase activity during Pi deprivation, leaf senescence, or salt stress was also abolished in this *atpap17* line; and (ii) there was no obvious up-regulation of any other intra- or extracellular HMW or LMW APase isozyme to compensate for the loss of *AtPAP17* expression.

Wang *et al.* (2014) reported that AtPAP17 knockout did not influence the up-regulation of total root or shoot APase activities during Pi deprivation, or the development or appearance of +Pi or –Pi *atpap17* shoots and roots during their cultivation on agar plates. We expanded this analysis to evaluate the growth and several biochemical parameters of *atpap17* plants growing in +Pi or –Pi media or soil, during leaf senescence, or following salinity stress. Consistent with the observations of Wang *et al.* (2014), there was no discernible alteration in the developmental or biochemical phenotype of *atpap17* plants under each of these conditions (Figs 8–10). No significant differences between *atpap17* and Col-0 seedlings were noted regarding the degree to which Pi deprivation increased total APase activity, root:shoot fresh weight ratio during cultivation on vertically oriented agar plates, or leaf anthocyanin content when grown in a –Pi soil mix under a regular light–dark regime (Fig. 8). In contrast, the analysis of Farhadi *et al.* (2020) of a comparable *atpap17* mutant (SALK_097940.47.75.x; also contains a T-DNA insertion in the last exon of the *AtPAP17* gene) indicated that relative to Col-0 controls, 21-day-old *atpap17* seedlings cultivated hydroponically under +Pi and –Pi conditions, respectively, exhibited: (i) a 31% increase and 10% decrease in fresh weight; and (ii) ~40% lower and 43% greater total APase activities. Their *atpap17* mutant seedlings were also reported as having 35% shorter and 20% longer roots when cultivated on vertically oriented +Pi versus –Pi agar plates, respectively, which also differs from the corresponding results of Wang *et al.* (2014) and the present study (Fig. 8A, E). The unexpected results that Farhadi *et al.* (2020) obtained with their *atpap17* mutant were attributed to the compensatory up-regulation of *AtPAP26* transcription, which was reported to increase by

~150% in the +Pi *atpap17* mutant relative to Col-0 plants, as determined by qRT-PCR with *ACTIN* as the reference gene. In contrast, qRT-PCR analysis failed to detect any significant alteration in *AtPAP26* expression in our +Pi *atpap17* mutant when either *ACTIN* or *TIP41* was employed as the reference gene (Supplementary Fig. S11A, B). Similarly, we observed no difference in *AtPAP26* expression in –Pi *atpap17* seedlings (relative to Col-0) when *TIP41* was the reference gene, whereas a marginal 1.2-fold increase in *AtPAP26* expression occurred with *ACTIN* as the reference gene (Supplementary Fig. S11A, B). Moreover, there was no obvious up-regulation of a HMW APase activity-staining band corresponding to the 100 kDa AtPAP26 homodimer (Veljanovski *et al.*, 2006; Hurley *et al.*, 2010; Robinson *et al.*, 2012*a*) following non-denaturing PAGE of intracellular or secretome extracts from our +Pi or –Pi *atpap17* plants relative to Col-0 controls (Fig. 4B). Farhadi *et al.* (2020) also described a large compensatory increase (i.e. >600%) in *AtPAP17* transcript abundance in an *atpap26* T-DNA mutant (SALK_152821) relative to Col-0 seedlings when cultivated under +Pi conditions. This contradicts the semi-quantitative RT-PCR analysis of Hurley *et al.* (2010) who did not detect any obvious alteration in *AtPAP17* transcript levels in shoots or roots of +Pi (or –Pi) seedlings of the same *atpap26* mutant line (SALK_152821) relative to Col-0 controls. There was also no difference apparent in the intensity of the LMW phosphatase activity-staining band corresponding to AtPAP17 that was observed following non-denaturing PAGE of extracts from –Pi *atpap26* versus Col-0 plants (Hurley *et al.*, 2010). Although our qRT-PCR analysis confirmed the results of Supplementary Fig. S4 (and numerous prior studies) that *AtPAP17* expression is greatly induced during Pi deprivation, there was no significant difference in *AtPAP17* mRNA abundance of +Pi or –Pi *atpap26* versus Col-0 plants when either *ACTIN* or *TIP41* was employed as the reference gene (Supplementary Fig. S11C, D). The reasons for the conspicuous discrepancies of current and prior *atpap17* and *atpap26* mutant studies with corresponding results of Farhadi *et al.* (2020) are unclear. Farhadi *et al.* (2020) also reported that complementation of their *atpap17* and *atpap26* plants with *AtPAP17* and *AtPAP26* genes, respectively, abolished all growth and biochemical phenotypes they reported for the mutants; this is difficult to evaluate, however, as the methods employed and results obtained with the respective complementation lines were not shown.

Leaves of soil-grown Col-0 and *atpap17* plants were fully expanded 21 d after planting and showed no phenotypic differences or signs of yellowing. Individual leaves were wrapped with aluminum foil to induce a senescence program that closely mimics natural senescence (Keech *et al.*, 2010; Robinson *et al.*, 2012*a*). The progression of senescence was monitored by observing the extent of leaf yellowing, as well as by assaying chlorophyll contents at various time points following initiation of prolonged darkness (Fig. 9A, B). Delayed senescence of Arabidopsis leaves occurred when the expression of senescence-associated genes encoding key hydrolytic enzymes such as a membrane lipase, RNase, or AtPAP26 was repressed or eliminated (Thompson *et al.*, 2000; He and Gan, 2002; Lers *et al.*, 2006; Robinson *et al.*, 2012*a*). This lag is thought to arise as a consequence of reduced macromolecule degradation, as the progress of senescence is tightly coordinated with the efficient recycling of nutrients freed by the catabolism of cellular macromolecules (Stigter and Plaxton, 2015). However, in contrast to the *atpap26* mutant (Robinson *et al.*, 2012*a*), there was no significant difference in the: (i) rate at which the senescing Col-0 and *atpap17* leaves yellowed or their chlorophyll contents decreased (Fig. 9A, B) or (ii) Pi remobilization efficiencies of fully senesced Col-0 and *atpap17* leaves which were determined to be 59±6% and 65±8% (means ±SE, of n=3 replicates), respectively. APase activities of clarified extracts prepared from *atpap17* and Col-0 leaves were also determined. Although leaf senescence triggered a marked increase in intracellular APase activity, which has been attributed to AtPAP26 up-regulation (Fig. 6A) (Robinson *et al.*, 2012*a*), no significant difference in extractable APase activity of non-senescing or senescing leaves of *atpap17* plants was detected relative to Col-0 controls (Fig. 9C).

Similarly, AtPAP17 loss of function exerted no obvious impact on appearance, shoot fresh or dry weights, or leaf APase or guaiacol PRx activities of 28-day-old soil-cultivated *atpap17* plants that had been irrigated with 150 mM NaCl for 1 week prior to harvest (Fig. 10A–C). Although APase activity of the clarified leaf extracts of *atpap17* plants was unaffected, guaiacol PRx activity uniformly increased by ~200% in leaves of the salt-stressed Col-0 and *atpap17* plants (Fig. 10C). Glutathione and ascorbate PRx up-regulation are well-established adaptations that contribute to ROS detoxification during plant acclimation to salinity stress (Ismail *et al.*, 2014). In contrast to our results (Fig. 10), a follow-up study to Farhadi *et al.* (2020) reported that when cultivated with 50–150 mM NaCl, *atpap17* mutant plants exhibited (relative to Col-0 controls) dramatic (i.e. up to ~50%) reductions in seedling fresh and dry weights, as well as total APase and guaiacol PRx activities of shoot or root extracts (Abbasi-Vineh *et al.*, 2021). Further investigations will be required to determine the reasons for the conflicting results of Farhadi *et al.* (2020) and Abbasi-Vineh *et al.* (2021) with those of Hurley *et al.* (2010), Wang *et al.* (2014), and the current study.

Secreted LMW AtPAP17 orthologs from common bean (PvPAP3), stylo (SgPAP7), and soybean (GmPAP7) were hypothesized to contribute to Pi scavenging from extracellular nucleoside triphosphates during Pi deprivation (Liang *et al.*, 2010; Liu *et al.*, 2016; Zhu *et al.*, 2020). As ATP was one of the better substrates utilized by purified AtPAP17 (Table 1), we also assessed whether the development of hydroponically cultivated *atpap17* plants might be compromised when 1 mM ATP was supplied as the sole source of exogenous P. However, the ATP-supplied Col-0 and *atpap17* plants grew just as well as +Pi plants, and there was no differences noted in their respective

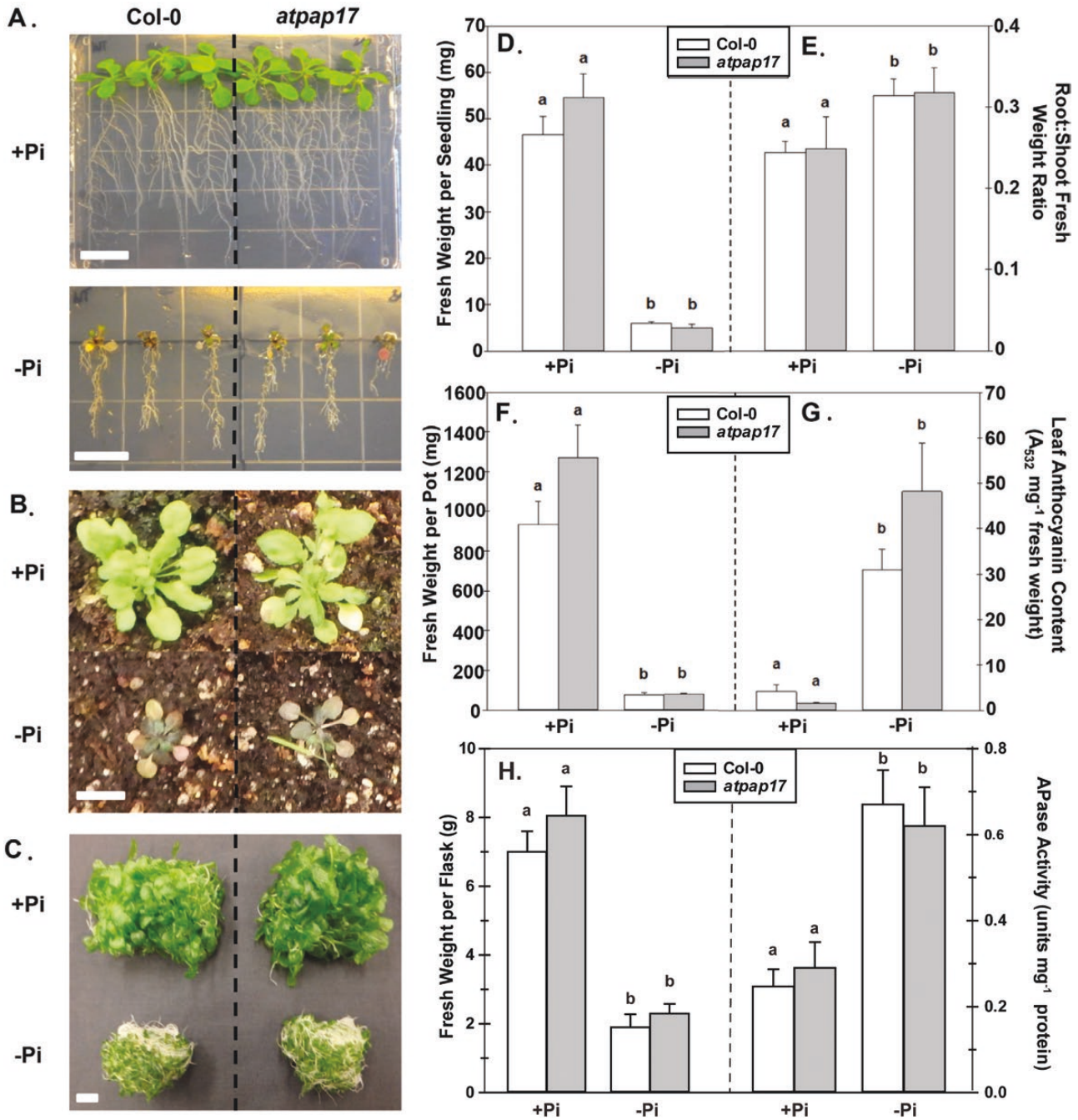

Fig. 8. AtPAP17 knockout does not impact the acclimation of Arabidopsis to Pi deprivation. +Pi and –Pi Col-0 and *atpap17* seedlings were cultivated: (A) on vertically oriented agar-solidified 0.5× Murashige and Skoog media plates for 14 d, (B) in a peat moss/perlite soil mixture for 21 d, or (C) in liquid 0.5× Murashige and Skoog medium for 14 d, as described in the Materials and methods. All images shown in (A–C) are representative of at least n=15 replicates; scale bar=1 cm. (D and E) The fresh weight per seedling (D) and root:shoot fresh weight ratio (E) of seedlings grown on +Pi or –Pi Murashige and Skoog media plates as shown in (A); all values represent means ±SE of n=15 replicates. (F and G) Rosette fresh weight per pot (F) and leaf anthocyanin content (G) of plants cultivated for 21 d on a soluble Pi-deficient soil mix that had been irrigated with +Pi or –Pi nutrient solutions as shown in (B); values represent means ±SE of n=10 biological replicates, where four plants made up each replicate. (F) The fresh weight per flask of 14-day-old seedlings grown hydroponically in +Pi and –Pi liquid Murashige and Skoog medium as described in the Materials and methods. All values represent means ±SE of n=4 biological replicates; different letters indicate statistically significant differences (P<0.05).

appearance or biomass (Supplementary Fig. S12). Previous research demonstrated that the secreted HMW AtPAP12 and AtPAP26 paralogs allow Arabidopsis to effectively exploit exogenous Po compounds such as glycerol-3-P, glucose-6-P, or purified herring sperm DNA as alternative sources of exogenous P nutrition (Robinson *et al.*, 2012*b*).

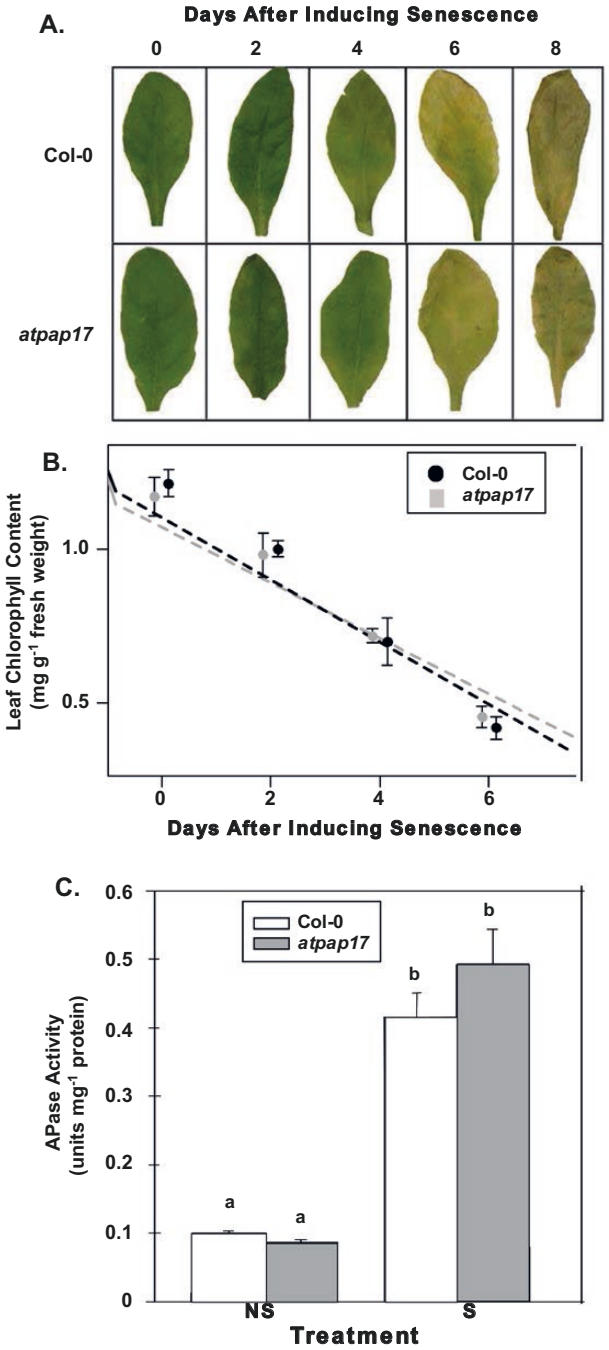

Fig. 9. AtPAP17 knockout does not influence the rate of senescence, chlorophyll content, or up-regulation of APase activity by senescing leaves. (A) Col-0 and *atpap17* plants were cultivated for 21 d in a standard soil mixture, and individual leaves in the fifth or sixth position were wrapped in foil sleeves for up to 8 d to induce senescence. Images shown are representative of at least 10 replicates each. (B) Chlorophyll content of Col-0 and *atpap17* leaves was determined at various times following the induction of leaf senescence. Dotted lines illustrate the rate of chlorophyll degradation as determined by linear regression. (C) APase activities were determined for clarified extracts of non-senescent (NS) and senescing (S) leaves. All values in (B) and (C) represent means ±SE of n=4 biological replicates; different letters indicate statistically significant differences (P<0.05).

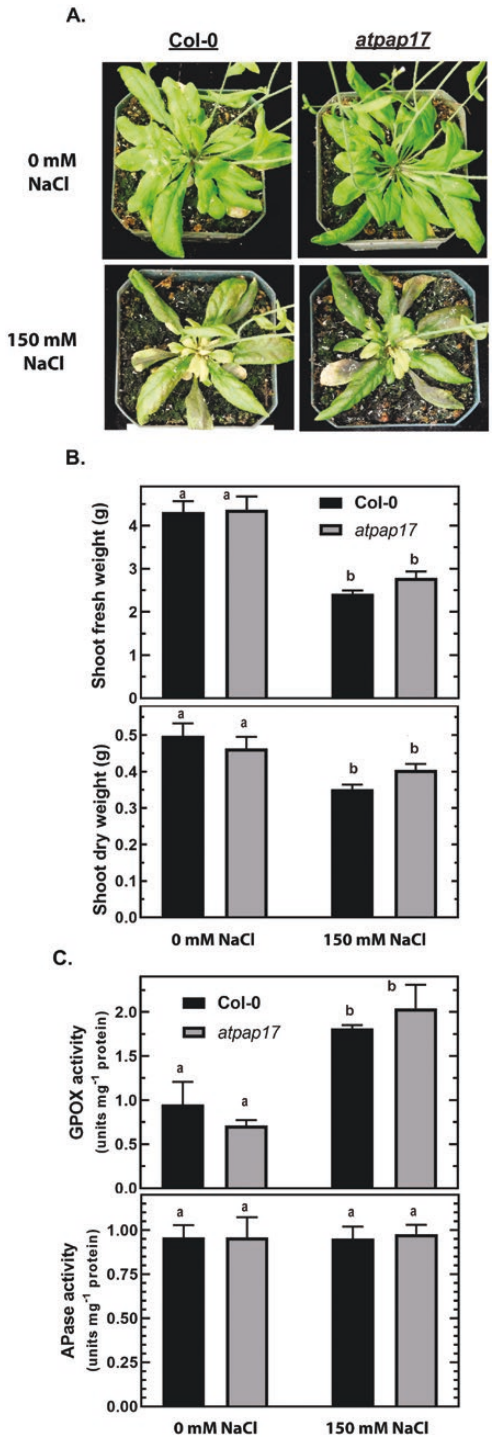

Fig. 10. AtPAP17 knockout does not influence the appearance, growth, or total APase or guaiacol PRx activities of salt-stressed, soil-cultivated plants. Col-0 and *atpap17* seedlings were established on agar-solidified nutrient plates for 7 d, then transferred to soil and cultivated in a growth cabinet under a regular fertilization and 16 h:8 h light:dark regime for an additional 21 d as described in the Materials and methods. The 28-day-old plants were irrigated with and without 150 mM NaCl for 1 week prior to harvest. Images shown in (A) are representative of at least 10 replicates. Shoot fresh and dry weights (B), and extractable guaiacol PRx (GPOX) and APase activities of clarified extracts prepared from fully expanded leaves (C) were also determined. All values in (B) and (C) represent means ±SE of duplicate determinations performed with n=4 biological replicates; different letters indicate statistically significant differences (P<0.05).

Discussion

The present study described the purification and characterization of AtPAP17 from the CW proteome of –Pi Arabidopsis suspension cells. We established that *de novo* AtPAP17 synthesis occurred in Arabidopsis suspension cells and seedlings responding to Pi deprivation or salinity stress, as well as in senescing leaves, whereas AtPAP17 was rapidly turned over following Pi resupply to –Pi cells or seedlings (Figs 4, 6). It is remarkable that AtPAP17 was the most significantly down-regulated of >1000 intracellular proteins whose abundance significantly changed 48 h following resupply of 2 mM Pi to the –Pi Arabidopsis cells (Mehta *et al.*, 2021). This parallels the rapid repression of *AtPAP17* transcription (i.e. within 30 min) that follows Pi resupply to –Pi Arabidopsis suspension cells or seedlings (del Pozo *et al.*, 1999; Müller *et al.*, 2004; Veljanovski *et al.*, 2006). A similar relationship between protein and transcript abundance has been reported for AtPAP12 and AtPAP25, HMW AtPAPs that are also up-regulated and secreted into the extracellular matrix of –Pi Arabidopsis (Tran *et al.*, 2010*b*; Del Vecchio *et al.*, 2014; Wang *et al.*, 2014). The overall results support the view that AtPAP17 up-regulation during Pi deprivation is controlled mainly at the transcriptional level since the *AtPAP17* promoter contains a binding site for PHR1, a transcription factor that functions as a master controller of the PSR (Bustos *et al.*, 2010). Mehta *et al.* (2021) also identified several intracellular proteases whose abundance significantly increased following Pi resupply to the –Pi Arabidopsis suspension cells, whereas the Pi resupply-mediated turnover of a pair of secreted, PSI HMW PAP isozymes of tomato suspension cells was correlated with the *de novo* synthesis and secretion of a pair of serine protease isoforms (Bozzo *et al.*, 2004*b*). Additional studies are needed to determine the identities, regulation, and mechanism of Pi resupply-inducible proteases that target PSI enzymes, including PAPs, for degradation. Stable overexpression of PSI proteins such as AtPAP17 in transgenic plants could be enhanced by modified protease expression and/or the design of protease-resistant PSI proteins.

Our results also demonstrated that AtPAP17 is dual-localized to the cell vacuole and extracellular matrix during Pi deprivation (Figs 4, 5), as occurs with AtPAP26 and its interacting lectin AtGAL1 (Hurley *et al.*, 2010; Ghahremani *et al.*, 2019*a*). This corroborates a study that listed AtPAP17 (i.e. At3g17790) as one of 370 different proteins identified in the CW proteome of rosettes of Arabidopsis plants that had been cultivated at 15 °C (Duruflé *et al.*, 2019). Although several other members of the LMW plant PAP family are also up-regulated and dual-localized during Pi deprivation, none has been localized to the cell vacuole (Liang *et al.*, 2010; Kataya *et al.*, 2016; Liu *et al.*, 2016; Zhu *et al.*, 2020). For example: (i) AtPAP7 is a LMW AtPAP17 paralog (Supplementary Fig. S1) localized to the endoplasmic reticulum and peroxisomes of Arabidopsis leaves (Kataya *et al.*, 2016); (ii) the LMW GmPAP7a and GmPAP7b paralogs of –Pi soybean were localized to the cytoplasm, plasma membrane, and apoplast when expressed in tobacco leaf epidermal cells (Zhu *et al.*, 2020); (iii) PvPAP3, the predominant LMW PAP up-regulated by –Pi bean plants, was localized to the plasma membrane and apoplast (Liang *et al.*, 2010); whereas (iv) SgPAP7, a LMW PAP up-regulated by –Pi *Stylosanthes*, localized to the plasma membrane and cytoplasm when expressed in bean roots (Liu *et al.*, 2016).

AtPAP17 appears to be a non-specific phosphatase as it exhibited widespread selectivity with various P-monoester and anhydride substrates (Tables 1, 2), similar to many previously characterized PAPs (Tran *et al.*, 2010*a*). However, the enzyme's broad pH phosphatase activity optima (Fig. 7A) differ from the vast majority of characterized plant PAPs, which generally display a much sharper pH activity profile with optimal activity centered around pH 5.5–6.0 (Tran *et al.*, 2010*a*). However, PvPAP3 also exhibited broad pH phosphatase activity optima in the range of pH 5.5–8.0 (Liang *et al.*, 2010), indicating that this might be a unique kinetic feature of LMW plant PAPs. This unusual property could facilitate their Pi-scavenging ability during: (i) alkalinization of the extracellular matrix that occurs during salinity or drought stress, or leaf senescence; or (ii) loss of tonoplast integrity that occurs during programmed cell death that accompanies senescence, and vacuolar proteins such as AtPAP17 become exposed to higher pH values characteristic of the cytoplasm (Geilfus, 2017; Borniego *et al.*, 2020).

As AtPAP17 also hydrolyzed Pi from phosphoamino acids and the phosphoprotein phosvitin (Table 1) it will also be of interest to assess its potential contribution to CW phosphoproteome reprogramming following stresses that trigger AtPAP17 up-regulation and accumulation in the extracellular matrix. Extracellular protein phosphorylation is widespread in animal and plant cells (Supplementary Fig. S3D) (Ghahremani and Plaxton, 2020), and HsACP5, the 36 kDa human ortholog of AtPAP17 (Supplementary Fig. S1), plays a key role in bone metabolism by dephosphorylating a secreted bone matrix phosphoprotein known as osteopontin (Schenk *et al.*, 2013). Similarly, CW-localized plant PAPs such as AtPAP25 or NtPAP12 of tobacco appear to function in signaling and/or CW metabolism by dephosphorylating CW phosphoproteins (Del Vecchio *et al.*, 2014; Ghahremani and Plaxton, 2020).

The induction of AtPAP17 by numerous stresses combined with the broad distribution of AtPAP17-like, LMW PAPs in phylogenetically diverse species implies an important and conserved function for AtPAP17 orthologs within the plant kingdom. Nevertheless, our careful analysis of a homozygous *atpap17* mutant failed to detect any biochemical or phenotypical changes associated with AtPAP17 loss of function during Pi deprivation, leaf senescence, or salinity stress (Figs 8–10). This corroborates results of Wang *et al.* (2014), and is likely to be due to the presence of other members of the AtPAP family, particularly AtPAP26, a highly expressed vacuolar and secreted HMW PAP that plays a dominant role in Pi scavenging and recycling during Pi deprivation or leaf senescence

(Veljanovski *et al.*, 2006; Hurley *et al.*, 2010; Tran *et al.*, 2010*b*; Robinson *et al.*, 2012*a*, *b*; Wang *et al.*, 2014; Ghahremani *et al.*, 2019*a*). In contrast, the PRx activity of AtPAP17, as well as several HMW plant PAPs including GmPAP3, was hypothesized to contribute to ROS detoxification during stress (del Pozo *et al.*, 1999; Liao *et al.*, 2003; Li *et al.*, 2008). Owing to superoxide and hence H_2O_2 generation as toxic byproducts of the photosynthetic and respiratory electron transport chains, ROS accumulates during stresses such as Pi deprivation or excessive salinity that trigger AtPAP17 up-regulation (Malusa *et al.*, 2002; Mittler, 2002; Ismail *et al.*, 2014). Because H_2O_2 readily diffuses through aquaporins, H_2O_2 produced at a specific site rapidly accumulates in other areas of the cell, including compartments where AtPAP17 is localized, namely the cell vacuole and extracellular matrix (Mittler, 2002). del Pozo *et al.* (1999) hypothesized that the PRx activity of AtPAP17 might contribute to ROS scavenging during oxidative stress that accompanies excessive salinity or drought, Pi deprivation, or treatment with H_2O_2. However, an important H_2O_2 metabolism role for AtPAP17 is difficult to reconcile with its relatively low V_{max} and affinity for H_2O_2 (Fig. 7B), coupled with the absence of phenotypic changes in the salt-stressed *atpap17* mutant relative to Col-0 control plants (Fig. 10). It is also important to recognize that H_2O_2 metabolism via a PAP's Fenton reaction does not scavenge ROS, as suggested by several studies (del Pozo *et al.*, 1999; Liao *et al.*, 2003; Li *et al.*, 2008), but is actually a ROS-generating process that produces highly reactive hydroxyl radicals (Fig. 1). Furthermore, stresses that induce AtPAP17 also induce a wide assortment of ROS-scavenging enzymes, including glutathione and ascorbate PRxs that exhibit a high activity and affinity for H_2O_2, and that are localized to all of the major compartments of plant cells, including the cell vacuole, CW, and apoplast (Mittler, 2002). A significant ROS-scavenging role for AtPAP17 during Pi deprivation is also difficult to reconcile with transcriptomic studies that have documented a host of PSI Arabidopsis genes involved in cell defense and oxidative stress amelioration (Morcuende *et al.*, 2007), as well as proteomic approaches that identified numerous intracellular and secreted antioxidant enzymes up-regulated by –Pi Arabidopsis (including glutathione reductase, dehydroascorbate reductase, superoxide dismutase, and several peroxidases) (Tran and Plaxton, 2008; Mehta *et al.*, 2021).

Concluding remarks

AtPAP17's unique expression profiles, dual-localization to CW/apoplast and cell vacuole, broad substrate selectivity and pH phosphatase activity profile, potent feedback inhibition by Pi, and rapid repression and turnover following Pi resupply to –Pi cells is indicative of its role in specialized metabolic pathways. Since AtPAP17 exhibits phosphoamino acid and protein phosphatase activity (Table 1), and extracellular protein phosphorylation has been well documented in plants (Supplementary Fig. S3D) (Ghahremani and Plaxton, 2020), a similar role for this enzyme cannot be discounted. Nevertheless, no significant phenotypic changes were detected during Pi deprivation, salinity stress, or leaf senescence of the *atpap17* T-DNA insertional mutant that we examined (Figs 8–10). It is clear that despite significant efforts and advances, further investigations will be required before our understanding of the biochemistry, biological functions, and regulation of LMW mammalian-type PAPs such as AtPAP17 will be complete. Overall, these studies are applicable to applied efforts to bioengineer Pi-efficient crops, urgently needed to reduce the overuse of non-renewable and polluting Pi-containing fertilizers in agriculture.

Supplementary data

The following supplementary data are available at *JXB* online.

Table S1. Primers used for cloning and PCR.

Table S2. AtPAP17 identification via MALDI-TOF MS peptide mass fingerprinting.

Table S3. Protein accession numbers of several AtPAP17 orthologs and their predicted molecular mass and location.

Table S4. Effect of various substances on AtPAP17 activity.

Fig. S1. Classification of Arabidopsis and human PAPs based on clustering analysis of deduced amino acid sequences.

Fig. S2. The optimized method for extracting and processing the soluble intracellular and CW proteomes of Arabidopsis suspension cells.

Fig. S3. SDS–PAGE of an intracellular and CW extract was followed by immunoblotting or multiplex phosphoprotein and total protein staining.

Fig. S4. *AtPAP17* is strongly induced following nutritional Pi deprivation of Arabidopsis seedlings or suspension cells.

Fig. S5. Heat map of the impact of various abiotic stresses on *AtPAP1-29* transcript abundance in Arabidopsis shoots and roots.

Fig. S6. AtPAP17 is immunologically distinct from Group I, HMW PAPs purified from CW extracts of –Pi Arabidopsis cell cultures.

Fig. S7. Estimation of AtPAP17's native molecular mass by analytical gel filtration FPLC.

Fig. S8. Deduced amino acid sequence alignment of NtPAP, AtPAP15, and AtPAP17.

Fig. S9. Relationship between protein concentration and PRx activity of AtPAP17 and HRP.

Fig. S10. Confirmation of T-DNA insert location in the *atpap17-2* mutant (SALK_085340) studied by Wang *et al.* (2014).

Fig. S11. The relative expression of *AtPAP26* and *AtPAP17* in Col-0, *atpap17*, and *atpap26* seedlings was determined with respect to the reference genes *ACTIN* and *TIP41*.

Fig. S12. AtPAP17 knockout does not influence appearance or growth of Arabidopsis seedlings supplied with 1.5 mM Pi or 1 mM ATP as their sole source of exogenous P.

Acknowledgements

We are grateful to Professor Dong Liu (Tsinghua University) for providing *atpap17* mutant seeds, and to Professor George diCenzo (Queen's University) for use of the Synergy H1 Microplate Reader.

Author contributions

BO'G, MG, KS, EW, AL, GM, MP, RM: performing the experiments; WP and BO'G: writing and assembling the manuscript with input by all co-authors.

Funding

This work was funded by Discovery, and Research Tool and Infrastructure grants from the Natural Science and Engineering Research Council of Canada (NSERC) (to WCP and RTM), the Queens's and Guelph Research Chair program (to WCP and RTM), and the U.S. National Science Foundation (to GCM). MG was the recipient of an Ontario Trillium Scholarship.

Data availability

All data supporting the findings of this study are available within the paper and within its supplementary data published online.

References

Abbasi-Vineh MA, Sabet MS, Karimzadeh G. 2021. Identification and functional analysis of two purple acid phosphatases AtPAP17 and AtPAP26 involved in salt tolerance in *Arabidopsis thaliana* plant. Frontiers in Plant Science **11**, 618716.

Akimoto K, Shinmen Y, Sumida M, Asami S, Amachi T, Yoshizumi H, Saeki Y, Shimizu S, Yamada H. 1990. Luminol chemiluminescence reaction catalyzed by a microbial peroxidase. Analytical Biochemistry **189**, 182–185.

Borniego ML, Molina MC, Guiamét JJ, Martinez DE. 2020. Physiological and proteomic changes in the apoplast accompany leaf senescence in *Arabidopsis*. Frontiers in Plant Science **10**, 1635.

Bozzo GG, Raghothama KG, Plaxton WC. 2002. Purification and characterization of two secreted purple acid phosphatase isozymes from phosphate-starved tomato (*Lycopersicon esculentum*) cell cultures. European Journal of Biochemistry **269**, 6278–6286.

Bozzo GG, Raghothama KG, Plaxton WC. 2004*a*. Structural and kinetic properties of a novel purple acid phosphatase from phosphate-starved tomato (*Lycopersicon esculentum*) cell cultures. The Biochemical Journal **377**, 419–428.

Bozzo GG, Singh VK, Plaxton WC. 2004*b*. Phosphate or phosphite addition promotes the proteolytic turnover of phosphate-starvation inducible tomato purple acid phosphatase isozymes. FEBS Letters **573**, 51–54.

Bustos R, Castrillo G, Linhares F, Puga MI, Rubio V, Pérez-Pérez J, Solano R, Leyva A, Paz-Ares J. 2010. A central regulatory system largely controls transcriptional activation and repression responses to phosphate starvation in Arabidopsis. PLoS Genetics **6**, e1001102.

Curtis MD, Grossniklaus U. 2003. A gateway cloning vector set for high-throughput functional analysis of genes in planta. Plant Physiology **133**, 462–469.

del Pozo JC, Allona I, Rubio V, Leyva A, de la Peña A, Aragoncillo C, Paz-Ares J. 1999. A type 5 acid phosphatase gene from *Arabidopsis thaliana* is induced by phosphate starvation and by some other types of phosphate mobilising/oxidative stress conditions. The Plant Journal **19**, 579–589.

Del Vecchio HA, Ying S, Park J, Knowles VL, Kanno S, Tanoi K, She YM, Plaxton WC. 2014. The cell wall-targeted purple acid phosphatase AtPAP25 is critical for acclimation of *Arabidopsis thaliana* to nutritional phosphorus deprivation. The Plant Journal **80**, 569–581.

Dissanayaka DMSB, Ghahremani M, Siebers M, Wasaki J, Plaxton WC. 2021. Recent insights into the metabolic adaptations of phosphorus-deprived plants. Journal of Experimental Botany **72**, 199–223.

Duruflé H, Ranocha P, Balliau T, Dunand C, Jamet E. 2019. Transcriptomic and cell wall proteomic datasets of rosettes and floral stems from five *Arabidopsis thaliana* ecotypes grown at optimal or sub-optimal temperature. Data in Brief **27**, 104581.

Ek-Rylander B, Barkhem T, Ljusberg J, Ohman L, Andersson KK, Andersson G. 1997. Comparative studies of rat recombinant purple acid phosphatase and bone tartrate-resistant acid phosphatase. The Biochemical Journal **321**, 305–311.

Farhadi S, Sabet MS, Malboobi MA, Moieni A. 2020. The critical role of AtPAP17 and AtPAP26 genes in Arabidopsis phosphate compensation network. Frontiers in Plant Science **11**, 565865.

Feder D, McGeary RP, Mitić N, Lonhienne T, Furtado A, Schulz BL, Henry RJ, Schmidt S, Guddat LW, Schenk G. 2020. Structural elements that modulate the substrate specificity of plant purple acid phosphatases: avenues for improved phosphorus acquisition in crops. Plant Science **294**, 110445.

Flanagan JU, Cassady AI, Schenk G, Guddat LW, Hume DA. 2006. Identification and molecular modeling of a novel, plant-like, human purple acid phosphatase. Gene **377**, 12–20.

Geilfus CM. 2017. The pH of the apoplast: dynamic factor with functional impact under stress. Molecular Plant **10**, 1371–1386.

Ghahremani M, Park J, Anderson EM, Marty-Howard NJ, Mullen RT, Plaxton WC. 2019*a*. Lectin AtGAL1 interacts with high-mannose glycoform of the purple acid phosphatase AtPAP26 secreted by phosphate-starved *Arabidopsis*. Plant, Cell & Environment **42**, 1158–1166.

Ghahremani M, Plaxton WC. 2020. Phosphoprotein phosphatase function of secreted purple acid phosphatases. In: Pandey GK, ed. Protein phosphatases and stress management in plants. Cham: Springer, 11–28.

Ghahremani M, Stigter KA, Plaxton WC. 2016. Extraction and characterization of extracellular proteins and their post-translational modifications from *Arabidopsis thaliana* suspension cell cultures and seedlings: a critical review. Proteomes **4**, 25.

Ghahremani M, Tran H, Biglou SG, O'Gallagher B, She YM, Plaxton WC. 2019*b*. A glycoform of the secreted purple acid phosphatase AtPAP26 co-purifies with a mannose-binding lectin (AtGAL1) upregulated by phosphate-starved Arabidopsis. Plant, Cell & Environment **42**, 1139–1157.

Hayman AR, Cox TM. 1994. Purple acid-phosphatase of the human macrophage and osteoclast—characterization, molecular-properties, and crystallization of the recombinant di-iron-oxo protein secreted by baculovirus-infected insect cells. Journal of Biological Chemistry **269**, 1294–1300.

He Y, Gan S. 2002. A gene encoding an acyl hydrolase is involved in leaf senescence in Arabidopsis. The Plant Cell **14**, 805–815.

Hurley BA, Tran HT, Marty NJ, Park J, Snedden WA, Mullen RT, Plaxton WC. 2010. The dual-targeted purple acid phosphatase isozyme AtPAP26 is essential for efficient acclimation of Arabidopsis to nutritional phosphate deprivation. Plant Physiology **153**, 1112–1122.

Ismail A, Takeda S, Nick P. 2014. Life and death under salt stress: same players, different timing? Journal of Experimental Botany **65**, 2963–2979.

Kataya AR, Schei E, Lillo C. 2016. Towards understanding peroxisomal phosphoregulation in *Arabidopsis thaliana*. Planta **243**, 699–717.

Keech O, Pesquet E, Gutierrez L, Ahad A, Bellini C, Smith SM, Gardeström P. 2010. Leaf senescence is accompanied by an early disruption of the microtubule network in Arabidopsis. Plant Physiology **154**, 1710–1720.

Knowles VL, Plaxton WC. 2013. Quantification of total and soluble inorganic phosphate. Bio-Protocol **3**, doi: 10.21769/BioProtoc.890

Lers A, Sonego L, Green PJ, Burd S. 2006. Suppression of LX ribonuclease in tomato results in a delay of leaf senescence and abscission. Plant Physiology **142**, 710–721.

Li D, Zhu H, Liu K, Liu X, Leggewie G, Udvardi M, Wang D. 2002. Purple acid phosphatases of *Arabidopsis thaliana*. Comparative analysis and differential regulation by phosphate deprivation. Journal of Biological Chemistry **277**, 27772–27781.

Li WF, Shao G, Lam HM. 2008. Ectopic expression of GmPAP3 alleviates oxidative damage caused by salinity and osmotic stresses. New Phytologist **178**, 80–91.

Liang C, Tian J, Lam HM, Lim BL, Yan X, Liao H. 2010. Biochemical and molecular characterization of PvPAP3, a novel purple acid phosphatase isolated from common bean enhancing extracellular ATP utilization. Plant Physiology **152**, 854–865.

Liao H, Wong FL, Phang TH, Cheung MY, Li WY, Shao G, Yan X, Lam HM. 2003. *GmPAP3*, a novel purple acid phosphatase-like gene in soybean induced by NaCl stress but not phosphorus deficiency. Gene **318**, 103–111.

Liu PD, Xue YB, Chen ZJ, Liu GD, Tian J. 2016. Characterization of purple acid phosphatases involved in extracellular dNTP utilization in *Stylosanthes*. Journal of Experimental Botany **67**, 4141–4154.

Malusa E, Laurenti E, Juszczuk I, Ferrari RP, Rychter AM. 2002. Free radical production in roots of *Phaseolus vulgaris* subjected to phosphate deficiency stress. Plant Physiology and Biochemistry **40**, 963–967.

Mehta D, Ghahremani M, Pérez-Fernández M, Tan M, Schläpfer P, Plaxton WC, Uhrig RG. 2021. Phosphate and phosphite have a differential impact on the proteome and phosphoproteome of Arabidopsis suspension cell cultures. The Plant Journal **105**, 924–941.

Mittler R. 2002. Oxidative stress, antioxidants and stress tolerance. Trends in Plant Science **7**, 405–410.

Morcuende R, Bari R, Gibon Y, *et al.* 2007. Genome-wide reprogramming of metabolism and regulatory networks of Arabidopsis in response to phosphorus. Plant, Cell & Environment **30**, 85–112.

Müller R, Nilsson L, Krintel C, Nielsen TH. 2004. Gene expression during recovery from phosphate starvation in roots and shoots of *Arabidopsis thaliana*. Physiologia Plantarum **122**, 233–243.

Murashige T, Skoog F. 1962. A revised medium for rapid growth and bio assays with tobacco tissue cultures. Physiologia Plantarum **15**, 473–497.

Olczak M, Olczak T. 2007. N-glycosylation sites of plant purple acid phosphatases important for protein expression and secretion in insect cells. Archives of Biochemistry and Biophysics **461**, 247–254.

Rio DC, Ares M Jr, Hannon GJ, Nilsen TW. 2010. Purification of RNA using TRIzol (TRI Reagent). Cold Spring Harbor Protocols **2010**, doi: 10.1101/pdb.prot5439.

Robinson WD, Carson I, Ying S, Ellis K, Plaxton WC. 2012*a*. Eliminating the purple acid phosphatase AtPAP26 in *Arabidopsis thaliana* delays leaf senescence and impairs phosphorus remobilization. New Phytologist **196**, 1024–1029.

Robinson WD, Park J, Tran HT, Del Vecchio HA, Ying S, Zins JL, Patel K, McKnight TD, Plaxton WC. 2012*b*. The secreted purple acid phosphatase isozymes AtPAP12 and AtPAP26 play a pivotal role in extracellular phosphate-scavenging by *Arabidopsis thaliana*. Journal of Experimental Botany **63**, 6531–6542.

Schenk G, Guddat LW, Ge Y, Carrington LE, Hume DA, Hamilton S, de Jersey J. 2000. Identification of mammalian-like purple acid phosphatases in a wide range of plants. Gene **250**, 117–125.

Schenk G, Mitić N, Hanson GR, Comba P. 2013. Purple acid phosphatase: a journey into the function and mechanism of a colorful enzyme. Coordination Chemistry Reviews **257**, 473–482.

Shane MW, Stigter K, Fedosejevs ET, Plaxton WC. 2014. Senescence-inducible cell wall and intracellular purple acid phosphatases: implications for phosphorus remobilization in *Hakea prostrata* (Proteaceae) and *Arabidopsis thaliana* (Brassicaceae). Journal of Experimental Botany **65**, 6097–6106.

Stigter KA, Plaxton WC. 2015. Molecular mechanisms of phosphorus metabolism and transport during leaf senescence. Plants **4**, 773–798.

Sun L, Wang L, Zheng Z, Liu D. 2018. Identification and characterization of an Arabidopsis phosphate starvation-induced secreted acid phosphatase as a vegetative storage protein. Plant Science **277**, 278–284.

Thompson J, Taylor C, Wang TW. 2000. Altered membrane lipase expression delays leaf senescence. Biochemical Society Transactions **28**, 775–777.

Tran HT, Hurley BA, Plaxton WC. 2010*a*. Feeding hungry plants: the role of purple acid phosphatases in phosphate nutrition. Plant Science **179**, 14–27.

Tran HT, Plaxton WC. 2008. Proteomic analysis of alterations in the secretome of *Arabidopsis thaliana* suspension cells subjected to nutritional phosphate deficiency. Proteomics **8**, 4317–4326.

Tran HT, Qian W, Hurley BA, She YM, Wang D, Plaxton WC. 2010*b*. Biochemical and molecular characterization of AtPAP12 and AtPAP26: the predominant purple acid phosphatase isozymes secreted by phosphate-starved *Arabidopsis thaliana*. Plant, Cell & Environment **33**, 1789–1803.

Veljanovski V, Vanderbeld B, Knowles VL, Snedden WA, Plaxton WC. 2006. Biochemical and molecular characterization of AtPAP26, a vacuolar purple acid phosphatase up-regulated in phosphate-deprived Arabidopsis suspension cells and seedlings. Plant Physiology **142**, 1282–1293.

Wang L, Li Z, Qian W, *et al.* 2011. The Arabidopsis purple acid phosphatase AtPAP10 is predominantly associated with the root surface and plays an important role in plant tolerance to phosphate limitation. Plant Physiology **157**, 1283–1299.

Wang L, Liu D. 2018. Functions and regulation of phosphate starvation-induced secreted acid phosphatases in higher plants. Plant Science **271**, 108–116.

Wang L, Lu S, Zhang Y, Li Z, Du X, Liu D. 2014. Comparative genetic analysis of *Arabidopsis* purple acid phosphatases AtPAP10, AtPAP12, and AtPAP26 provides new insights into their roles in plant adaptation to phosphate deprivation. Journal of Integrative Plant Biology **56**, 299–314.

Xu SL, Medzihradszky KF, Wang ZY, Burlingame AL, Chalkley RJ. 2016. N-Glycopeptide profiling in Arabidopsis inflorescence. Molecular & Cellular Proteomics **15**, 2048–2054.

Yang ZM, Chen Y, Hu BY, Tan ZQ, Huang BT. 2015. Identification and validation of reference genes for quantification of target gene expression with quantitative real-time PCR for tall fescue under four abiotic atresses. PLoS One **10**, e0119569.

Zhu SN, Chen MH, Liang CY, Xue YB, Lin SL, Tian J. 2020. Characterization of purple acid phosphatase family and functional analysis of GmPAP7a/7b involved in extracellular ATP utilization in soybean. Frontiers in Plant Science **11**, 661.